

Using pre-formed Meisenheimer complexes as dopants for n-type organic thermoelectrics with high Seebeck coefficients and power factors

*Jinfeng Han¹, Connor Ganley², Qin Hu^{3,4}, Xingang Zhao¹, Paulette Clancy², Thomas P. Russell^{3,4}, Howard E. Katz¹, **

J. Han, X. Zhao, Prof. H. E. Katz

¹Department of Materials Science and Engineering and Department of Chemistry, Johns Hopkins University, Baltimore, Maryland 21218, United States.

Email: hekatz@jhu.edu

C. Ganley, Prof. P. Clancy

²Department of Chemical and Biomolecular Engineering, Johns Hopkins University, Baltimore, Maryland 21218, United States.

Q. Hu, Prof. T. P. Russell

³Polymer Science and Engineering Department, University of Massachusetts, Amherst, Massachusetts 01003, United States

⁴Materials Sciences Division, Lawrence Berkeley National Laboratory, Berkeley, California 94720, United States

Keywords: complex dopant, n-type polymer thermoelectrics, high Seebeck coefficient, high power factor.

Abstract:

A pre-formed Meisenheimer complex of an NDI with TBAF was obtained in a simple way by mixing dibrominated NTCDI and tetrabutylammonium fluoride (TBAF) in solution and used as dopant for *n*-type organic thermoelectrics. Two *n*-type polymers PNDICITVT and PBDOPVTT were synthesized, *n*-doped, and characterized as conductive and thermoelectric materials. PNDICITVT doped with NDI-TBAF presents a high σ value of 0.20 S cm⁻¹, a Seebeck Coefficient, *S*, of -1854 μ V K⁻¹ and a power factor (*PF*) of 67 μ W m⁻¹ K⁻², among the highest reported *PF* in solution-processed

conjugated *n*-type polymer thermoelectrics. Using N-DMBI and NDI-TBAF as co-dopants, PNDICITVT has a $PF > 35 \mu\text{W m}^{-1} \text{K}^{-2}$; while for PBDOPVTT $\sigma = 0.75 \text{ S cm}^{-1}$ and $PF = 58 \mu\text{W m}^{-1} \text{K}^{-2}$. In this work, we found that an ionic adduct together with a neutral dopant improved the performance of *n*-type organic thermoelectrics leading to an enhanced power factor, and more generally, we also elucidated the role of such an adduct in polymer doping.

Introduction:

Organic semiconducting materials have found a broad range of applications, including commercially, as organic light-emitting diodes (OLEDs), organic field effect transistors (OFETs) and photovoltaic devices.^[1] Dopants at low concentrations have been shown to improve semiconductor performance in such devices,^[2] for example by promoting charge injection into OLEDs and filling traps to increase mobility in OFETs, as will be discussed below. There is renewed and increasing interest in the design of conjugated polymer-dopant systems to produce printable, flexible, optoelectronic, and bio-active electronic conductors.^[3] Organic conductors are also attracting increased attention for low-temperature thermoelectric applications.^[4] Conjugated polymers offer a number of advantages in that they are lightweight, and solution-processable, have low thermal conductivity, an improved low-temperature thermoelectric performance ($< 200 \text{ }^{\circ}\text{C}$), and a natural mechanical flexibility. As a result, conjugated polymers are promising materials for current and near future wearable electronics.^[5]

The power factor, PF , is usually used to assess the thermoelectric performance. It can be calculated from the following equation:

$$PF = S^2 \sigma \quad (1)$$

where S is the Seebeck coefficient ($\mu\text{V K}^{-1}$) and σ is electrical conductivity (S cm^{-1}). Because conjugated polymers generally have similar values of thermal conductivity, improving the electrical conductivity and Seebeck coefficient will effectively enhance thermoelectric performance. The electrical conductivity of the most conductive p -type polymers is on the order of hundreds to thousands of S cm^{-1} , and the power factor is usually tens to hundreds of $\mu\text{W/m K}^2$.^[4a, 6] Compared to p -type organic thermoelectric materials, n -type organic thermoelectric materials usually exhibit lower values of σ and S , resulting in a lower PF .

Several approaches have been explored to improve the power factor of n -type organic thermoelectrics. Huang *et al.* developed a quinoid molecule with a high PF of $236 \mu\text{W m}^{-1} \text{K}^{-2}$ at 373 K, demonstrating a powerful strategy to achieve high performance organic thermoelectrics.^[7] For n -type polymer thermoelectrics backbone engineering is an effective way to improve σ or S . Lei and coworkers designed and synthesized a pyrazine-flanked DPP-based polymer, with a short π - π stacking distance of 3.38 Å, that presented a high PF of $57 \mu\text{W m}^{-1} \text{K}^{-2}$.^[8] These studies typically used 4-(1,3-Dimethyl-2,3-dihydro-1H-benzimidazol-2-yl)phenyl)dimethylamine (N-DMBI) as the dopant, and the polymer synthesis process is not straightforward. Most n -type polymer

thermoelectrics have PF values below $30 \mu\text{W m}^{-1} \text{K}^{-2}$ and breakthroughs are difficult to achieve.^[5a, 9] This provides an incentive to introduce novel n -type dopants to meet the demand of improved electron transport in organic semiconducting films.^[10] Previously, we used tetrabutylammonium fluoride (TBAF) as a polymer dopant to prepare thermoelectric devices, yielding $\sigma = 0.62 \text{ S cm}^{-1}$.^[11] Pei *et al.* reported a new dopant, triaminomethane (TAM), for n -type polymer thermoelectrics and reported a high PF of $51 \mu\text{W m}^{-1} \text{K}^{-2}$.^[12] Recently, devices with improved electron mobility (up to $1.1 \text{ cm}^2 \text{V}^{-1} \text{s}^{-1}$) were achieved by doping N2200 (poly[N,N'-bis(2-octyldodecyl)-naphthalene-1,4,5,8-bis(dicarboximide)-2,6-diyl]-alt-5,5'-(2,2'-bithiophene) with an adduct, (12a,18a)-5,6,12,12a,13,18,18a,19-octahydro-5,6-dimethyl-13,18[1',2']-benzenobisbenzimidazo [1,2-b:2',1'-d]benzo[*i*][2.5]benzodiazocine potassium triflate (DMBI-BDZC).^[13]

In some of the examples mentioned above, dopants are used that do not seem to be plausible single-electron acceptors or donors, even though they show dopant activity. Tris(pentafluorophenyl)borane ($\text{B}(\text{C}_6\text{F}_5)_3$) was used with conjugated polymers and their molecular semiconductor blends, not in order to reach a high σ value, but rather to increase the field-effect transistor mobility, possibly by oxidizing traps.^[14] In another case, a substantial σ was achieved in poly(3-hexylthiophene) doped with $\text{B}(\text{C}_6\text{F}_5)_3$.^[15] Kao *et al.* showed that fluoroalkyltrichlorosilanes were extremely effective dopants to make high- σ polythiophenes, but the authors argued that the doping mechanism involved protons generated by hydrolysis of the silanes.^[16] This is consistent with

statements in a recent publication about $(\text{B}(\text{C}_6\text{F}_5)_3)$ that $(\text{B}(\text{C}_6\text{F}_5)_3)$ does not act as an oxidant, but instead reacts with water to form a Brønsted acid, whose proton forms a covalent adduct with a mildly Lewis basic polymer that serves as a dopant for another polymer chain.^[17] Doping by the strong acid bis(trifluoromethanesulfonyl)imide of the sterically hindered poly(3-(2-ethylhexyl)thiophene) was found to be two orders of magnitude better as a dopant than tetrafluorotetracyanoquinodimethane (F_4TCNQ).^[18] Thomas *et al.* stated,^[19] “For acidic dopants, it is postulated that the carbocation generated from backbone protonation oxidizes a neighboring chain, leading to the traditional radical-hole pair and the associated Brønsted base.” There are multiple references to the general use of small anions (even F^-) as dopants for fullerenes and other small molecules,^[20] but there is some question as to whether F^- could act as an electron donor,^[21] making it more likely that fluoro-Meisenheimer complexes formed *in situ* from F^- and polymer subunits could be electron donors for other polymer chains.

In this paper, using NTCDI and TBAF as raw materials, we developed pre-formed Meisenheimer complexes of NDI-TBAF as *n*-type dopants from a dibrominated NDI + TBAF using a simple mixing method. The NMR spectrum of NDI-TBAF is shown in the Supporting Information.^[21b] We synthesized a new polymer, PNDICITVT, based on a weak donor unit dichlorodithienylethene (CITVT) by Stille coupling in ortho-dichlorobenzene (*o*-DCB) (**Figure 1a**). PBDOPVTT was synthesized by Stille coupling PNDICITVT in chlorobenzene (**Figure 1a**). The M_w values of PNDICITVT and PBDOPVTT are 154 and 116 kDa, respectively, and the corresponding polydispersity

indices (PDIs) are 3.7 and 1.3. PNDICITVT doped with NDI-TBAF shows a high σ of 0.20 S cm^{-1} , comparable to films doped with N-DMBI, and a much higher S of $-1854 \text{ } \mu\text{V K}^{-1}$. This results in an improved PF of $67 \text{ } \mu\text{W m}^{-1} \text{ K}^{-2}$ (10 wt%). This is also the first demonstration of a pre-formed Meisenheimer complex showing doping capabilities, supporting the above hypothesis. To improve the performance stability of NDI-TBAF-based devices, N-DMBI and 5 wt% NDI-TBAF were used as co-dopants, creating a doped polymer that displays a high PF , exceeding $35 \text{ } \mu\text{W m}^{-1} \text{ K}^{-2}$ at the N-DMBI ratio of 30 mol% and 50 mol%. To demonstrate the value of co-dopants to improve performance, we prepared thermoelectric devices based on doped PBDOPVTT, obtaining a high σ value of 0.75 S cm^{-1} (50 mol% N-DMBI and 5 wt% NDI-TBAF) and a PF near $60 \text{ } \mu\text{W m}^{-1} \text{ K}^{-2}$ at a N-DMBI ratio of 50 mol% and 75 mol%. To the best of our knowledge, this PF value is one of the highest known power factors of n -type donor-acceptor (D-A) polymers (**Figure 1b**),^[8, 9b-e, 11-12, 22] suggesting an enhancement resulting from co-dopants and the additional advantage in using Meisenheimer complexes for n -type polymer thermoelectrics. We used *ab initio* density functional theory calculations of key molecular structures and their electronic properties to help evaluate the mechanism by which such complexes promote n -type polymer conductivity.

Experimental Results:

NDI-TBAF (mole ratio:1/1) was prepared by mixing NTCDI and TBAF (1 M in THF) in a glove box (N_2 , $\text{H}_2\text{O} < 6 \text{ ppm}$, $\text{O}_2 < 0.1 \text{ ppm}$) and made up as a solution in THF with

a total concentration of 2.5 mg/mL. NDI-TBAF has previously been studied.,^[21b] The color of the NDI-TBAF mixed solution is red, readily distinguishing it from the color of NTCDI (faint yellow) and TBAF (colorless) (Figure S10). The ¹H NMR spectra of NDI-TBAF shows that the environment of hydrogen atoms in the NDI is altered by the addition of TBAF.

As described in more detail in the Supporting Information, PNDICITVT was synthesized by coupling NDI-2Br with a weak donor of CITVT. PBDOPVTT is an *n*-type polymer based on dichlorinated BDOPV and bithiophene.^[23] A pristine film of PNDICITVT has a maximal, low-energy absorption peak at 647 nm with a smaller shoulder peak at 712 nm; no obvious absorption was observed beyond 850 nm (**Figure 2a**). PNDICITVT doped with 5 wt% NDI-TBAF presents stronger absorption than the pristine polymer film and the absorption spectra can be detected beyond 850 nm, suggesting PNDICITVT can be successfully *n*-doped by NDI-TBAF. When the ratio of NDI-TBAF was increased to 10 wt%, the absorption at 550-750 nm is much stronger than that doped with 5 wt%; however, absorption beyond 850 nm is weaker (**Figure 2a**). The two absorption peaks between 600 nm and 750 nm became a single broad peak when PNDICITVT was doped with 5 wt% NDI-TBAF and 30 mol% N-DMBI. When N-DMBI was increased to 100 mol%, the absorption spectra beyond that region is much stronger than that doped with 30 mol% N-DMBI (**Figure 2a**). PBDOPVTT doped with NDI-TBAF has weaker polaron absorption than PNDICITVT, too small to be observed readily by the absorption spectroscopy, suggesting that PNDICITVT can be more easily

doped by NDI-TBAF (**Figure 2b**) and this is consistent with the higher conductivity observed for PNDICITVT-NDI-TBAF, discussed below. The LUMO energy levels of PNDICITVT and PBDOPVTT are similar, around -3.90 eV, and the HOMO energy level of PBDOPVTT (-5.55 eV) is slightly lower than that of PNDICITVT (-5.47 eV). The LUMO and HOMO energy levels of PNDICITVT and PBDOPVTT doped with 5 wt% NDI-TBAF are -3.81/-5.54 eV and -3.91/-5.50 eV, respectively, nearly the same as for the undoped cases (**Figure 2c, d**). The result also shows that PNDICITVT can be more easily doped by NDI-TBAF than can PBDOPVTT. The EPR spectra of intrinsic and doped PNDICITVT and PBDOPVTT indicate that both of them can be doped by the preassembled complex (**Figure 2e and 2f**).

We measured the thermoelectric properties of doped polymers in the open air. The thickness of the polymer films is about 300-400 nm. The doped polymer films remained stable during the measurement process. PNDICITVT doped with 10 wt% NDI-TBAF showed a maximum conductivity of 0.20 S cm^{-1} (**Figure 3a**). This result shows an enhancement in the conductivity from 0.006 to 0.2 S cm^{-1} as the NDI-TBAF ratio was increased from 0.5 wt% to 10 wt% (**Figure 3a**). Due to the established negative correlation between the Seebeck coefficient and charge carrier concentration, the corresponding Seebeck coefficient decreased from -3900 to $-1850 \text{ } \mu\text{V K}^{-1}$ (**Figure 3d**). The PF value improved from $9.2 \text{ } \mu\text{W m}^{-1} \text{ K}^{-2}$ (0.5 wt%) to $67 \text{ } \mu\text{W m}^{-1} \text{ K}^{-2}$ (10 wt%), which is among the highest power factors yet observed in *n*-type solution-processed conjugated polymer thermoelectrics (**Figure 1a and 3d**). The high PF associated with

NDI-TBAF could be associated, we believe, with the creation of an electronic energy level, either on one NDI molecule or within an aggregate, that is located slightly below the transport level once an electron is donated from NDI-TBAF to the polymer. It is also possible that NDI subunits fit among polymer segments to improve the intermolecular interactions that promote mobility, so the conductivity-Seebeck coefficient tradeoff is decreased, and fewer charge carriers need be generated to achieve a given conductivity increase. We also cannot rule out that the high Seebeck coefficient could include an ionic thermogalvanic, or energy filtering contribution,^[24] as discussed below. N-DMBI, which was developed by the Bao group, can promote hydrogen- and/or electron-transfer reactions via radical formation and is known to play a key role in recent *n*-type organic thermoelectrics.^[25] A maximum value of $\sigma = 0.11 \text{ S cm}^{-1}$ was obtained when PNDICITVT was doped with 50 mol% N-DMBI (**Figure 3b**). When the N-DMBI ratio increased from 5 mol% to 75 mol%, the Seebeck coefficient of doped PNDICITVT decreased from -770 to $-310 \text{ } \mu\text{V K}^{-1}$ (**Figure 3e**). If the N-DMBI ratio is increased to 100 mol%, S became positive, producing a value of $146 \text{ } \mu\text{V K}^{-1}$. The S value of PNDICITVT doped with N-DMBI is far below that doped with NDI-TBAF and their σ values are close, resulting in a much lower PF of $2.6 \text{ } \mu\text{W m}^{-1} \text{ K}^{-2}$ (**Figure 3e**). A very high *n*-type power factor was also found^[26] using inorganic CuCl_2 as a binding metal and an anion source in a possibly hydrated (PEDOT:PSS) medium. This would normally be expected to conduct holes, making it likely that their high power factors arise via a different mechanism.

Though the maximum value for the PF of PNDICITVT doped with NDI-TBAF is very high, we found that the performance was not very consistent, perhaps due to a transient contribution to S . To decrease this possibility, we created thermoelectric devices with 5 wt% NDI-TBAF and various fractions of N-DMBI as co-dopants. When the N-DMBI ratio is 75 mol%, doped PNDICITVT exhibited the maximum σ of 0.12 S cm^{-1} . Even when the N-DMBI ratio was reduced to 50 mol%, the σ remains close to 0.10 S cm^{-1} , suggesting that high σ values can be obtained in a broader range of N-DMBI fraction than when N-DMBI is the sole dopant (**Figure 3c**). The Seebeck coefficient decreased from -7200 to $-850 \text{ } \mu\text{V K}^{-1}$ when the N-DMBI ratio increased from 5 mol% to 100 mol% (**Figure 3f**). When the N-DMBI ratio is 50 mol%, doped PNDICITVT presented the highest PF of $36 \text{ } \mu\text{W m}^{-1} \text{ K}^{-2}$ (**Figure 3f**). Moreover, both PNDICITVT:5 wt% NDI-TBAF doped with 50 mol% and 75 mol% of N-DMBI showed high PF values above $35 \text{ } \mu\text{W m}^{-1} \text{ K}^{-2}$, which is much higher than that doped with a single N-DMBI dopant, showing the enhancement in performance due to the use of co-dopants (**Figure 3f**).

PBDOPVTT doped with NDI-TBAF presented the best σ value of 0.04 S cm^{-1} at a dopant weight ratio of 10 wt%, with corresponding values for S and PF of $-1640 \text{ } \mu\text{V K}^{-1}$ and $8.3 \text{ } \mu\text{W m}^{-1} \text{ K}^{-2}$, respectively (**Figure 4a, d**). The highest PF is $9.5 \text{ } \mu\text{W m}^{-1} \text{ K}^{-2}$ (5 wt%) due to the correspondingly high value of S of $-5216 \text{ } \mu\text{V K}^{-1}$ (**Figure 4d**). The best σ value of PBDOPVTT doped with N-DMBI is 8.1 S cm^{-1} (75 mol%) and the corresponding PF is $21 \text{ } \mu\text{W m}^{-1} \text{ K}^{-2}$ (**Figure 4b, e**), which is similar to that reported for other N-DMBI-doped n -type conjugated polymers.^[9d, 22c] Using 5 wt% NDI-TBAF and

varying the fraction of N-DMBI as co-dopants, we were able to create doped PBDOPVTT with a σ value of 0.75 S cm^{-1} (50 mol% N-DMBI), and corresponding S and PF values of $-870 \text{ } \mu\text{V K}^{-1}$ and $56 \text{ } \mu\text{W m}^{-1} \text{ K}^{-2}$, respectively (**Figure 4c, f**). The highest PF was $58 \text{ } \mu\text{W m}^{-1} \text{ K}^{-2}$ (75 mol% N-DMBI), which arises from a higher S value of $-960 \text{ } \mu\text{V K}^{-1}$. The PF is higher than that of previously reported n -type conjugated polymer thermoelectrics, suggesting the generality of using co-dopants to achieve high power factor n -type polymer thermoelectrics.

According to previous reports, σ follows an Arrhenius-type dependence of conductivity with temperature T , which can be determined by the equation:

$$\sigma_e = \sigma_{e,\infty} \exp\left(-\frac{E_A}{k_B T}\right) \quad (2)$$

where $\sigma_{e,\infty}$ is the theoretical maximal electrical conductivity, k_B is Boltzmann constant, T is temperature and E_A are the thermal activation energy.^[27] To understand how σ varies with temperature, σ values of PNDICITVT and PBDOPVTT doped with co-dopants were measured over a range of -10 to $260 \text{ } ^\circ\text{C}$ (an average of about 400 K). Both polymers exhibit a linear dependence of $\ln(\text{conductivity})$ versus reciprocal temperature (**Figure 5**). The thermal activation energy of carrier hopping is calculated to be 154 and 81 meV for PNDICITVT and PBDOPVTT, respectively. Dividing by 400 K yields a projected value for S of $200\text{-}400 \text{ } \mu\text{V/K}$, several times less than what was measured for the highest PF samples, indicating a contribution from an alternate mechanism such as ionic redistribution, a thermogalvanic effect, or energy filtering. It should be noted that the electroactivities of fluoride and TBA ions are minimal, making

a thermogalvanic effect based on those species unlikely. While it is outside the scope of this study to examine this issue in detail, it is possible that there is a temperature dependence of the stability of either or both of the ions in the organic media. Different adduct configurations could perhaps be more or less stable, depending on the temperature. However, the tetrabutylammonium ion may be too large to be transported in response to a small temperature gradient. The fluoride ions would need to “hop” between molecules, and forming adducts, in order to be preferentially distributed at the hot or cold ends. This would also slow their transport. Voltages induced by temperature differences showed no apparent transience over a time interval that would have been indicative of an ionic contribution (Supporting Information, Section 6). Energy filtering at the boundaries of crystalline domains remains a possibility.

The electron mobilities of pristine PNDICITVT and PBDOPVTT were evaluated to be 0.05 ± 0.01 and 0.09 ± 0.02 $\text{cm}^2 \text{V}^{-1} \text{s}^{-1}$, respectively; the on/off ratio of two polymers is about 2000 (Figure S2). The electron mobilities of PNDICITVT and PBDOPVTT doped with 0.05 wt% NDI-TBAF are 0.03 and 0.04 $\text{cm}^2 \text{V}^{-1} \text{s}^{-1}$, respectively, and the threshold voltage is much lower than that of pristine polymers (Figure S3a and S4a). This may be because the ions in THF disorder the molecular packing of polymer films. The electron mobilities of PNDICITVT and PBDOPVTT doped with 0.02 mol% N-DMBI are enhanced to be 0.09 and 0.4 $\text{cm}^2 \text{V}^{-1} \text{s}^{-1}$, respectively, which are much higher than that of the pristine polymers, especially for PBDOPVTT (Figure S3b and S4b).

Using 0.05 wt% NDI-TBAF and 0.02mol% N-DMBI as the co-dopants, electron mobility of 0.1 and 0.8 cm² V⁻¹ s⁻¹ were obtained for PNDICITVT and PBDOPVTT (Figure S3c and S4c), respectively, and they are higher than those of pristine polymers, doped with N-DMBI or doped with NDI-TBAF, showing the excellent performance of co-dopants. NDI-TBAF appears to provide higher Seebeck coefficients when used as the sole dopant, but it needs to be dissolved in THF in which the polymers are not readily dissolved. As a result, the performance of the resulting doped films is not very consistent. Using co-dopants we can take advantage of the high conductivity of N-DMBI doped films and high Seebeck coefficient associated with NDI-TBAF doping in more consistently prepared films.

Grazing incidence wide angle X-ray scattering shows that PBDOPVTT is more crystalline in the pristine film. The pristine PBDOPVTT presents an edge-on orientation, whereas PNDICITVT presents both edge-on and face-on orientations. The lamellar packing and π - π stacking distances were calculated to be 25.1 Å ($q = 0.251 \text{ Å}^{-1}$) and 3.63 Å ($q = 1.73 \text{ Å}^{-1}$) for PNDICITVT, while 31.4 Å ($q = 0.2 \text{ Å}^{-1}$) and 3.45 Å ($q = 1.82 \text{ Å}^{-1}$) for PBDOPVTT (Figure S5). PNDICITVT and PBDOPVTT doped with NDI-TBAF showed a higher degree of face-on π - π stacking than the pristine polymers, especially for PBDOPVTT. The π - π stacking distances were 3.59 Å ($q = 1.75 \text{ Å}^{-1}$) and 3.49 Å ($q = 1.8 \text{ Å}^{-1}$), respectively (Figure S5). Both PNDICITVT and PBDOPVTT doped with co-dopants have much weaker π - π stacking diffraction intensity, suggesting that the two different dopants may disorder the arrangement of molecules (**Figure 6b**).

Atomic force microscope (AFM) images suggest that PNDICITVT doped with NDI-TBAF or N-DMBI are homogeneous, perhaps related to the fact that films of PNDICITVT doped with NDI-TBAF, N-DMBI and co-dopants all have similar electrical conductivity (Figure S6). However, PBDOPVTT doped with N-DMBI shows better homogeneity than that doped with NDI-TBAF or co-dopants (Figure S7). If we can improve the miscibility of PBDOPVTT doped with NDI-TBAF, a higher conductivity might be achieved.

Computational Results:

To evaluate the possible role of adduct dopants in the electronic property enhancements described above, we simulated the electronic structures and calculated ionization potentials of representative dopant structures using density functional theory (DFT). We used the ORCA software package^[28] to model the components of the adduct and represented the acetonitrile as an “implicit solvent” (expressed as a mean field of a suitable dielectric constant). Details of the DFT methodology, parameters, and settings used in this computational investigation are provided in the Supporting Information. We uncovered three energetically preferred sites of complexation of a bare fluoride ion to the N,N-dimethyl NDI in our initial studies of a simplified system (**Figure 6**), with the strongest binding energy to the carbonyl carbons at around 0.2 eV. When we incorporated tetramethylammonium as a counterion in separate simulations, the binding energy increased to about 0.6 eV, *i.e.*, became stronger. The ionization energy of the

adduct with its counterion was calculated to be about 6.3 eV. Use of Cs^+ as a counterion gave a similar ionization energy, although -interestingly- it showed essentially no binding energy (comparable to that of the bare fluoride adduct complex), consistent with an unsuccessful attempt to observe that adduct by NMR. We also found that both the binding energy and ionization energy of the counterion systems were isotropic with respect to the counterion's position around the fluoride ion. The ionization energy is about 2 eV less than the likely electron affinities of the *n*-type polymers used in this paper. But those affinities do not account for the presence of the counterions, or the increased entropy resulting from the many more possible electronic configurations of doped polymers compared to the adducts. Most importantly, the ionization energies of tetramethylammonium and cesium fluorides are calculated to be 7.2 and 7.6 eV, respectively. This is a full eV higher than that of the adduct, making the adduct a much more likely source of *n*-doping than the pure fluoride salts. The binding energy is considerably higher than the activation for mobility, making fluoride transport an unlikely mechanism for the change in conductivity.

Conclusions:

We used pre-formed Meisenheimer complexes of NDI-TBAF as *n*-type dopants and showed their utility in achieving high Seebeck coefficients and power factors in *n*-type polymer thermoelectrics. PNDICITVT doped with NDI-TBAF presents a high power factor of $67 \mu\text{W m}^{-1} \text{K}^{-2}$. Using N-DMBI and NDI-TBAF as co-dopants, *PF* of 36 and $58 \mu\text{W m}^{-1} \text{K}^{-2}$ were achieved for PNDICITVT and PBDOPVTT, respectively. Our

results showed, for the first time, that F- incorporated as a Meisenheimer adduct, the form in which it may generally be present in *n*-type polymers, is active as an *n*-dopant and that this type of dopant can be used for high performance *n*-type organic thermoelectrics, including as a co-dopant with N-DMBI.

Supporting Information

Supporting Information is available from the Wiley Online Library or from the authors.

Acknowledgements

We thank Professor Patricia McGuiggan for assistance with AFM measurements. We also thank Dr. Tushita Mukhopadhyaya (Howard E. Katz group) and Garvin Peters (J.D. Tovar group) for their assistance with CV measurements, Arlene Chiu (Susanna Thon's group) for her help with UV-vis-NIR spectra measurements, and Baixiang Li for his help with GPC measurements. This work was primarily supported by the National Science Foundation, Division of Chemistry, grant number 1708245. Q. Hu and T. P. Russell were supported by the US Office of Naval Research under contract N00014-17-1-2241. GIWAXS were performed at beamline 7.3.3 of the Advanced Light Source, Lawrence Berkeley National Laboratory, which is supported by the DOE, Office of Science, and Office of Basic Energy Sciences.

Received: ((will be filled in by the editorial staff))

Revised: ((will be filled in by the editorial staff))

Published online: ((will be filled in by the editorial staff))

References:

- [1] a) S. Yuvaraja, A. Nawaz, Q. Liu, D. Dubal, S. G. Surya, K. N. Salama, P. Sonar, *Chem. Soc. Rev.* **2020**, *49*, 3423; b) A. Wadsworth, Z. Hamid, J. Kosco, N. Gasparini, I. McCulloch, *Adv. Mater.* **2020**, *32*, 2001763; c) S. Wang, H. Zhang, B. Zhang, Z. Xie, W.-Y. Wong, *Mat. Sci. Eng. R.* **2020**, *140*, 100547; d) S.-J. Zou, Y. Shen, F.-M. Xie, J.-D. Chen, Y.-Q. Li, J.-X. Tang, *Mater. Chem. Front.* **2020**, *4*, 788.
- [2] B. Lüssem, M. Riede, K. Leo, *Phys. Status Solidi A* **2013**, *210*, 9.
- [3] a) M. Bharti, A. Singh, S. Samanta, D. K. Aswal, *Prog. Mater. Sci.* **2018**, *93*, 270; b) C. J. Yao, H. L. Zhang, Q. Zhang, *Polymers-Basel* **2019**, *11*; c) S. Inal, J. Rivnay, A. O. Suiu, G. G. Malliaras, I. McCulloch, *Acc. Chem. Res.* **2018**, *51*, 1368; d) J. Liu, Y. Shi, J. Dong, M. I. Nugraha, X. Qiu, M. Su, R. C. Chiechi, D. Baran, G. Portale, X. Guo, L. J. A. Koster, *ACS Energy Lett.* **2019**, *4*, 1556; e) M. Moser, J. F. Ponder, A. Wadsworth, A. Giovannitti, I. McCulloch, *Adv. Funct. Mater.* **2018**, 29.
- [4] a) O. Bubnova, Z. U. Khan, A. Malti, S. Braun, M. Fahlman, M. Berggren, X. Crispin, *Nat. Mater.* **2011**, *10*, 429; b) B. Russ, A. Glaudell, J. J. Urban, M. L. Chabiny, R. A. Segalman, *Nat. Rev. Mater.* **2016**, *1*; c) S. Lee, S. Kim, A. Pathak, A. Tripathi, T. Qiao, Y. Lee, H. Lee, H. Y. Woo, *Macromol. Res.* **2020**, *28*, 531; d) M. Lindorf, K. A. Mazzio, J. Pflaum, K. Nielsch, W. Brütting, M. Albrecht, *J. Mater. Chem. A* **2020**, *8*, 7495.
- [5] a) R. M. Kluge, N. Saxena, W. Chen, V. Körstgens, M. Schwartzkopf, Q. Zhong, S. V. Roth, P. Müller-Buschbaum, *Adv. Funct. Mater.* **2020**, 2003092; b) T. Park, C. Park, B. Kim, H. Shin, E. Kim, *Energy Environ. Sci.* **2013**, *6*; c) S. Panigrahy, B. Kandasubramanian, *Eur. Polym. J.* **2020**, *132*; d) P. C. Y. Chow, T. Someya, *Adv. Mater.* **2020**, *32*, 1902045; e) W. Shi, Y. Guo, Y. Liu, *Adv. Mater.* **2020**, *32*, 1901493; f) M. Wang, P. Baek, A. Akbarinejad, D. Barker, J. Travas-Sejdic, *J. Mater. Chem. C* **2019**, *7*, 5534.
- [6] Y. Du, K. F. Cai, S. Chen, P. Cizek, T. Lin, *ACS Appl. Mater. Inter.* **2014**, *6*, 5735.
- [7] D. Huang, H. Yao, Y. Cui, Y. Zou, F. Zhang, C. Wang, H. Shen, W. Jin, J. Zhu, Y. Diao, W. Xu, C. A. Di, D. Zhu, *J. Am. Chem. Soc.* **2017**, *139*, 13013.
- [8] X. Yan, M. Xiong, J. T. Li, S. Zhang, Z. Ahmad, Y. Lu, Z. Y. Wang, Z. F. Yao, J. Y. Wang, X. Gu, T. Lei, *J. Am. Chem. Soc.* **2019**, *141*, 20215.
- [9] a) S. Wang, H. Sun, T. Erdmann, G. Wang, D. Fazzi, U. Lappan, Y. Puttison, Z. Chen, M. Berggren, X. Crispin, A. Kiriy, B. Voit, T. J. Marks, S. Fabiano, A. Facchetti, *Adv. Mater.* **2018**, *30*, e1801898; b) J. Liu, G. Ye, B. V. Zee, J. Dong, X. Qiu, Y. Liu, G. Portale, R. C. Chiechi, L. J. A. Koster, *Adv. Mater.* **2018**, *30*, e1804290; c) C. Y. Yang, W. L. Jin, J. Wang, Y. F. Ding, S. Nong, K. Shi, Y. Lu, Y. Z. Dai, F. D. Zhuang, T. Lei, C. A. Di, D. Zhu, J. Y. Wang, J. Pei, *Adv. Mater.* **2018**, *30*, e1802850; d) K. Shi, F. Zhang, C. A. Di, T. W. Yan, Y. Zou, X. Zhou, D. Zhu, J. Y. Wang, J. Pei, *J. Am. Chem. Soc.* **2015**, *137*, 6979; e) S. Wang, H. Sun, U. Ail, M. Vagin, P. O. Persson, J. W. Andreasen, W. Thiel, M. Berggren, X. Crispin, D. Fazzi, S. Fabiano, *Adv. Mater.* **2016**, *28*, 10764; f) O. Bardagot, P. Kubik, T. Marszalek, P. Veyre, A. A. Medjahed, M. Sandroni, B. Grévin, S. Pouget, T. Nunes Domschke, A. Carella, S. Gambarelli, W. Pisula, R. Demadrille, *Adv. Funct. Mater.* **2020**, *30*,

2000449.

- [10] D. Huang, C. Wang, Y. Zou, X. Shen, Y. Zang, H. Shen, X. Gao, Y. Yi, W. Xu, C. A. Di, D. Zhu, *Angew Chem. Int. Ed.* **2016**, *55*, 10672.
- [11] X. Zhao, D. Madan, Y. Cheng, J. Zhou, H. Li, S. M. Thon, A. E. Bragg, M. E. DeCoster, P. E. Hopkins, H. E. Katz, *Adv. Mater.* **2017**, *29*.
- [12] C. Y. Yang, Y. F. Ding, D. Huang, J. Wang, Z. F. Yao, C. X. Huang, Y. Lu, H. I. Un, F. D. Zhuang, J. H. Dou, C. A. Di, D. Zhu, J. Y. Wang, T. Lei, J. Pei, *Nat. Commun.* **2020**, *11*, 3292.
- [13] J. Panidi, J. Kainth, A. F. Paterson, S. Wang, L. Tsetseris, A. H. Emwas, M. A. McLachlan, M. Heeney, T. D. Anthopoulos, *Adv. Funct. Mater.* **2019**, *29*, 1902784.
- [14] a) Y. Han, G. Barnes, Y.-H. Lin, J. Martin, M. Al-Hashimi, S. Y. AlQaradawi, T. D. Anthopoulos, M. Heeney, *Chem. Mater.* **2016**, *28*, 8016; b) J. Panidi, A. F. Paterson, D. Khim, Z. Fei, Y. Han, L. Tsetseris, G. Vourlias, P. A. Patsalas, M. Heeney, T. D. Anthopoulos, *Adv. Sci.* **2018**, *5*, 1700290.
- [15] P. Pingel, M. Arvind, L. Kölln, R. Steyrleuthner, F. Kraffert, J. Behrends, S. Janietz, D. Neher, *Adv. Electron. Mater.* **2016**, *2*.
- [16] C. Y. Kao, B. Lee, L. S. Wielunski, M. Heeney, I. McCulloch, E. Garfunkel, L. C. Feldman, V. Podzorov, *Adv. Funct. Mater.* **2009**, *19*, 1906.
- [17] B. Yurash, D. X. Cao, V. V. Brus, D. Leifert, M. Wang, A. Dixon, M. Seifrid, A. E. Mansour, D. Lungwitz, T. Liu, P. J. Santiago, K. R. Graham, N. Koch, G. C. Bazan, T. Q. Nguyen, *Nat. Mater.* **2019**, *18*, 1327.
- [18] E. M. Thomas, E. C. Davidson, R. Katsumata, R. A. Segalman, M. L. Chabinyc, *ACS Macro Lett.* **2018**, *7*, 1492.
- [19] C. C. Han, Elsenbaumer, R. L., *Synthetic Met.* **1989**, *30*, 123.
- [20] a) C. Z. Li, C. C. Chueh, F. Ding, H. L. Yip, P. W. Liang, X. Li, A. K. Jen, *Adv. Mater.* **2013**, *25*, 4425; b) S. Torabi, J. Liu, P. Gordiichuk, A. Herrmann, L. Qiu, F. Jahani, J. C. Hummelen, L. J. Koster, *ACS Appl. Mater. Inter.* **2016**, *8*, 22623.
- [21] a) C. D. Weber, C. Bradley, M. C. Lonergan, *J. Mater. Chem. A* **2014**, *2*, 303; b) T. L. D. Tam, J. W. Xu, *Chem. Commun.* **2019**, *55*, 6225.
- [22] a) R. A. Schlitz, F. G. Brunetti, A. M. Glaudell, P. L. Miller, M. A. Brady, C. J. Takacs, C. J. Hawker, M. L. Chabinyc, *Adv. Mater.* **2014**, *26*, 2825; b) S. Hwang, W. J. Potscavage, Y. S. Yang, I. S. Park, T. Matsushima, C. Adachi, *Phys. Chem. Chem. Phys.* **2016**, *18*, 29199; c) W. Ma, K. Shi, Y. Wu, Z. Y. Lu, H. Y. Liu, J. Y. Wang, J. Pei, *ACS Appl. Mater. Inter.* **2016**, *8*, 24737; d) Y. Wang, K. Takimiya, *Adv. Mater.* **2020**, *32*, 2002060.
- [23] Y.-Q. Zheng, Z.-F. Yao, T. Lei, J.-H. Dou, C.-Y. Yang, L. Zou, X. Meng, W. Ma, J.-Y. Wang, J. Pei, *Adv. Mater.* **2017**, *29*, 1701072.
- [24] a) A. Mazaheripour, S. Majumdar, D. Hanemann-Rawlings, E. M. Thomas, C. McGuinness, L. d'Alencon, M. L. Chabinyc, R. A. Segalman, *Chem. Mater.* **2018**, *30*, 4816; b) D. Zhao, A. Martinelli, A. Willfahrt, T. Fischer, D. Bernin, Z. U. Khan, M. Shahi, J. Brill, M. P. Jonsson, S. Fabiano, X. Crispin, *Nat. Commun.* **2019**, *10*, 1093; c) A. K. K. Kyaw, G. D. H. Wong, T. A. Yemata, J. Xu, *Org. Electron.* **2019**, *69*, 7.
- [25] a) J. H. O. Peng Wei, Guifang Dong, Zhenan Bao, *J. Am. Chem. Soc.* **2010**, *132*, 8852; b) B. D. Naab, S. Guo, S. Olthof, E. G. Evans, P. Wei, G. L. Millhauser, A.

- Kahn, S. Barlow, S. R. Marder, Z. Bao, *J. Am. Chem. Soc.* **2013**, *135*, 15018; c) D. Kiefer, A. Giovannitti, H. Sun, T. Biskup, A. Hofmann, M. Koopmans, C. Cendra, S. Weber, L. J. Anton Koster, E. Olsson, J. Rivnay, S. Fabiano, I. McCulloch, C. Muller, *ACS Energy Lett.* **2018**, *3*, 278; d) L. Qiu, J. Liu, R. Alessandri, X. Qiu, M. Koopmans, Remco W. A. Havenith, S. J. Marrink, R. C. Chiechi, L. J. Anton Koster, J. C. Hummelen, *J. Mater. Chem. A* **2017**, *5*, 21234.
- [26] B. Kim, J. U. Hwang, E. Kim, *Energy Environ. Sci.* **2020**, *13*, 859.
- [27] a) M. Schwarze, C. Gaul, R. Scholz, F. Bussolotti, A. Hofacker, K. S. Schellhammer, B. Nell, B. D. Naab, Z. Bao, D. Spoltore, K. Vandewal, J. Widmer, S. Kera, N. Ueno, F. Ortmann, K. Leo, *Nat. Mater.* **2019**, *18*, 242; b) S. Olthof, S. Mehraeen, S. K. Mohapatra, S. Barlow, V. Coropceanu, J. L. Bredas, S. R. Marder, A. Kahn, *Phys. Rev. Lett.* **2012**, *109*, 176601.
- [28] a) F. Neese, *Wiley Interdiscip. Rev. Comput. Mol. Sci.* **2012**, *2*, 73. b) F. Neese, *Wiley Interdiscip. Rev. Comput. Mol. Sci.* **2018**, *8*.

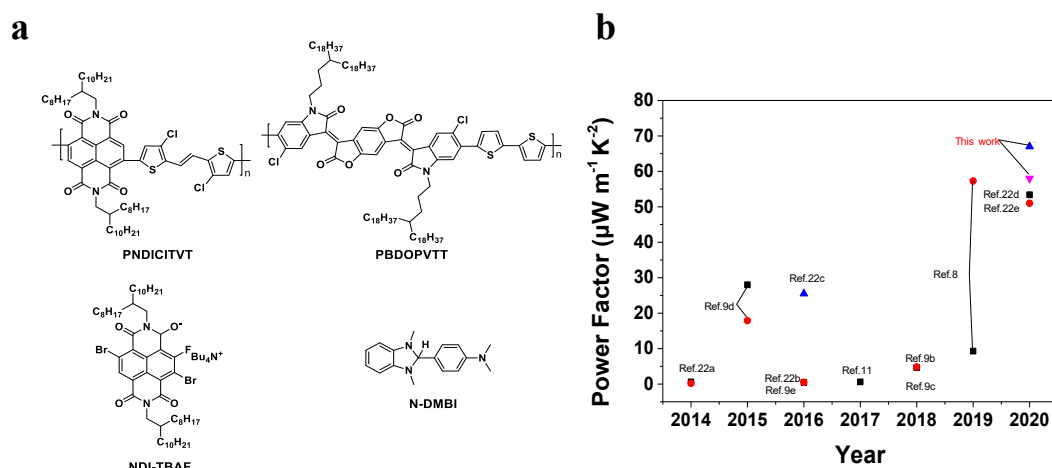


Figure 1. (a) The chemical structures of polymers and dopants used in this paper. (b) Power factors of reported papers and this work. NDI-TBAF is not pure and used as mixing complex for **n**-type organic thermoelectrics.

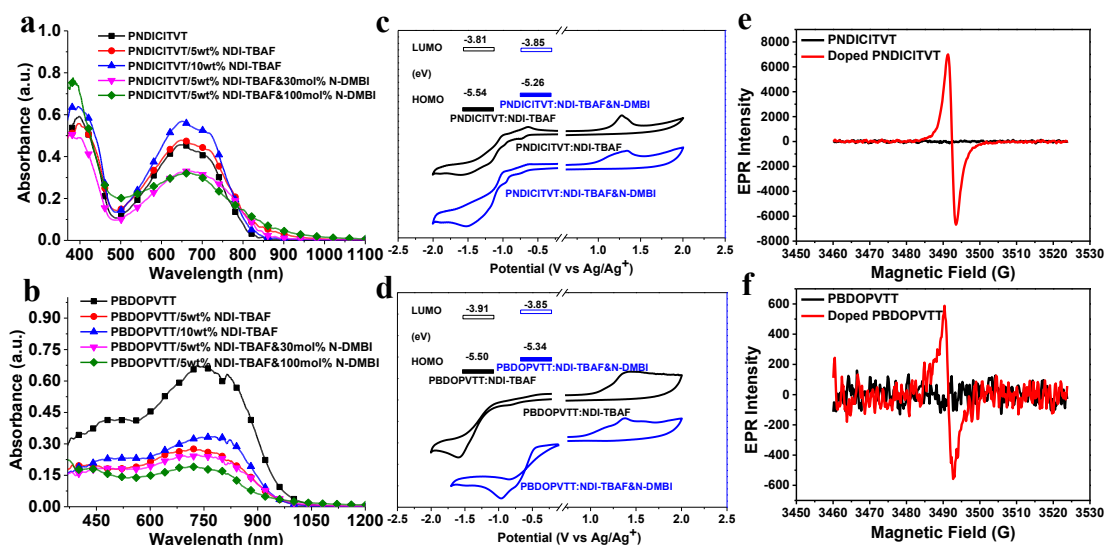


Figure 2. The UV-vis-NIR absorption spectra of (a) intrinsic and doped PNDICITVT and (b) intrinsic and doped PBDOPVTT polymer films. Cyclic voltammograms and energy levels of (c) doped PNDICITVT and (d) doped PBDOPVTT polymer films. EPR spectra of (e) intrinsic and doped PNDICITVT and (f) intrinsic and doped PBDOPVTT polymer films.

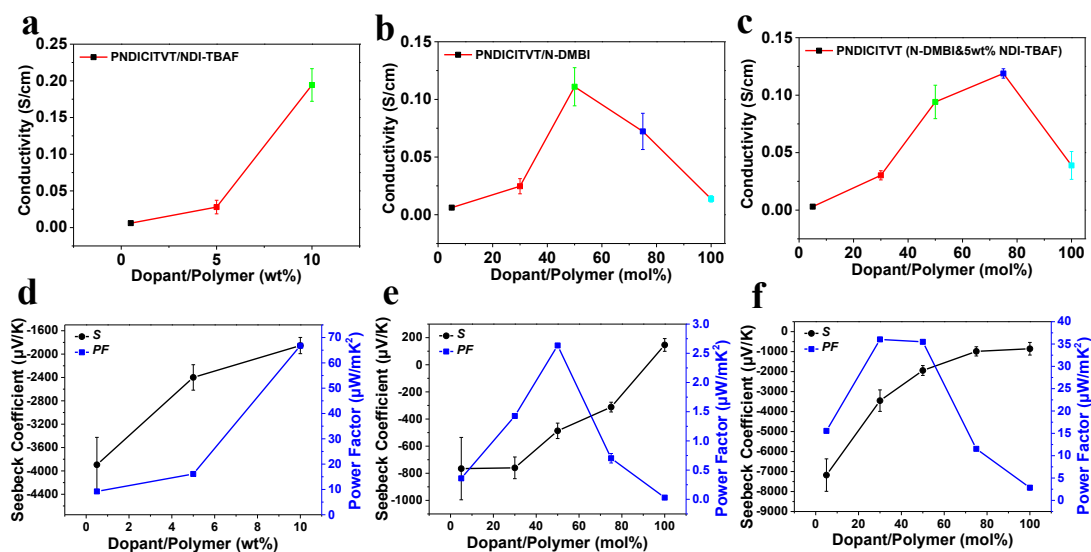


Figure 3. Electrical conductivity of PNDICITCT doped with (a) NDI-TBAF, (b) N-DMBI and (c) N-DMBI & 5 wt% NDI-TBAF. Seebeck coefficient and power factor of PNDICITCT doped with (d) NDI-TBAF, (e) N-DMBI and (f) N-DMBI & 5 wt% NDI-TBAF.

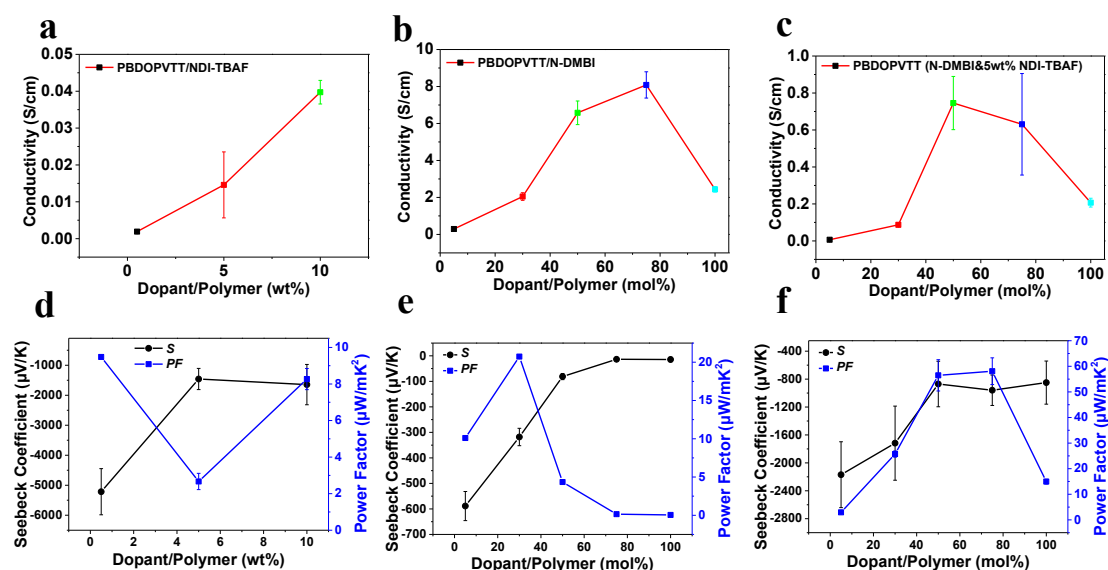


Figure 4. Electrical conductivity of PBDOPVTT doped with (a) NDI-TBAF, (b) N-DMBI and (c) N-DMBI & 5 wt% NDI-TBAF. Seebeck coefficient and power factor of PBDOPVTT doped with (d) NDI-TBAF, (e) N-DMBI and (f) N-DMBI & 5 wt% NDI-TBAF.

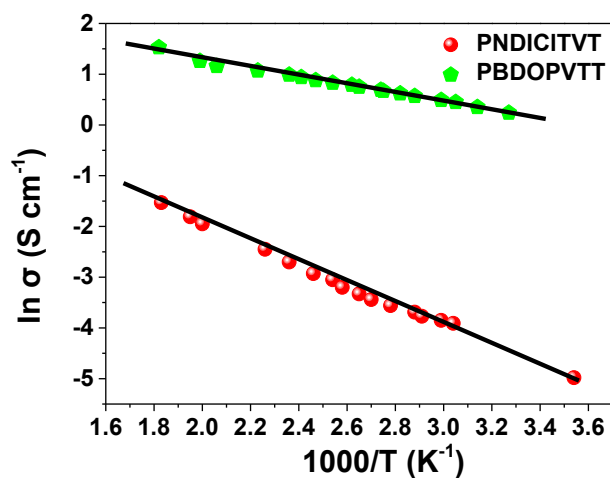


Figure 5. Temperature-dependent σ values of PNDICITVT and PBDOPVTT doped with co-dopants.

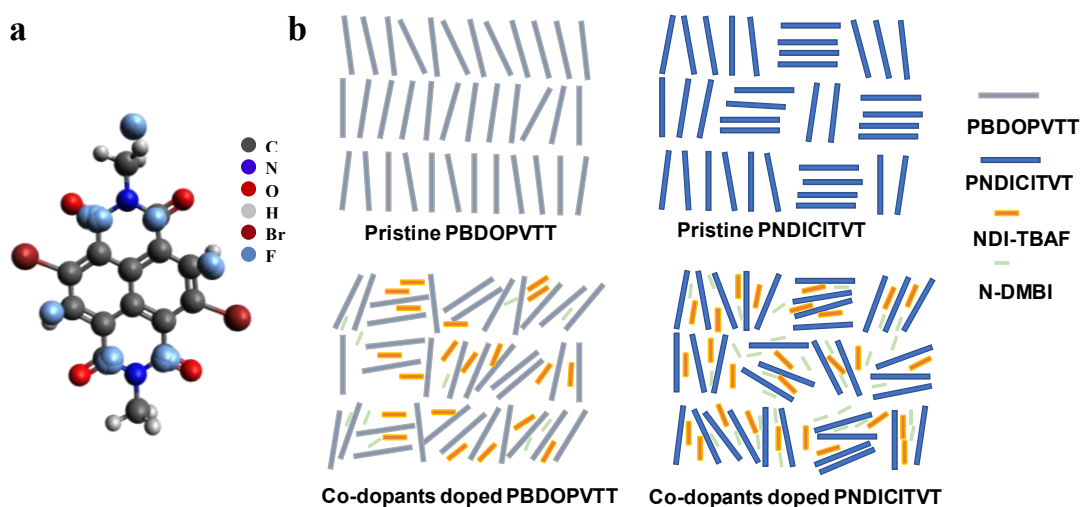


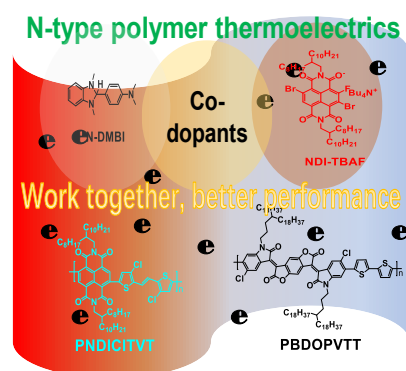
Figure 6. (a) Atomic-scale representation of the preferred locations for fluoride ion (pale blue) complexation above a representative motif of the N,N-dimethyl NDI backbone. (b) Schematic of molecular packing in pristine polymer films and doped polymer films.

Pre-formed Meisenheimer complexes of NDI-TBAF are obtained by mixing NTCDI and TBAF in solution and suitable for application in *n*-type organic thermoelectrics. NDI-TBAF doped PNDICITVT produces a PF of $67 \mu\text{W m}^{-1} \text{K}^{-2}$. Co-dopants of N-DMBI and NDI-TBAF-doped PNDICITVT and PBDOPVTT show high PF values of 35 and $58 \mu\text{W m}^{-1} \text{K}^{-2}$, respectively.

J. Han, C. Ganley, Q. Hu, X. Zhao, P. Clancy, T. P. Russell, H. E. Katz*

Using pre-formed Meisenheimer complexes as dopants for *n*-type organic thermoelectrics with high Seebeck coefficient and power factor

ToC figure



((Supporting Information can be included here using this template))

© Copyright 2020. WILEY-VCH GmbH.

Supporting Information

Using pre-formed Meisenheimer complexes as dopants for n-type organic thermoelectrics with high Seebeck coefficient and power factor

*Jinfeng Han¹, Connor Ganley², Qin Hu^{3,4}, Xingang Zhao¹, Paulette Clancy², Thomas P. Russell^{3,4}, Howard E. Katz^{1, *}*

J. Han, X. Zhao, Prof. H. E. Katz

¹Department of Materials Science and Engineering and Department of Chemistry, Johns Hopkins University, Baltimore, Maryland 21218, United States.

Email: hekatz@jhu.edu

C. Ganley, Prof. P. Clancy

²Department of Chemical and Biomolecular Engineering, Johns Hopkins University, Baltimore, Maryland 21218, United States.

Q. Hu, Prof. T.P. Russell

³Polymer Science and Engineering Department, University of Massachusetts, Amherst, Massachusetts 01003, United States

⁴Materials Sciences Division, Lawrence Berkeley National Laboratory, Berkeley, California 94720, United States

1. General procedures and experimental details.

Materials and Methods:

Chemical reagents (Including solvent and PMMA) were purchased and used as received. All the synthesis experiments were performed under N₂.

To make adduct-doped polymer solutions and films, 2 mg (2 mmol) of NDCTI-2Br was placed into a small glass bottle, the bottle was transferred to a glovebox, and 1 mL of anhydrous THF followed by 2 μ L TBAF solution (1 M in THF) were added. The bottle was shaken for 3 minutes. The total concentration of NDI-TBAF is 2.5 mg/mL. For conjugated polymer (4 mg/mL in o-DCB) doped with 5 wt% NDI-TBAF, 200 μ L polymer solution was added to a new small bottle, then 16 μ L NDI-TBAF solution was added and the mixture was heated at 75 °C for 1 min and stirred for 5 min. Then the solution was drop cast onto the substrate.

¹H and ¹³C NMR spectra were recorded on Bruker Advance (300 MHz/400 MHz) spectrometers. ¹H NMR chemical shifts were referenced to TMS (0 ppm), and ¹³C NMR chemical shifts were referenced to CDCl₃ (77.00 ppm). UV-vis-NIR absorption spectra were acquired using a spectrophotometer (Cary 50 UV/vis). Gel permeation chromatography (GPC) was performed on a PL gel MIXED-B LS 300 x 7.5mm x 3 at 150 °C using trichlorobenzene (TCB) stabilized with 0.0125% BHT as the eluent. Cyclic voltammetry (CV) was performed on a BASI Epsilon workstation. Thin films of polymers and doped polymers were analyzed in acetonitrile solutions under N₂ with 0.1 M tetrabutylammonium hexafluorophosphate (NBu₄PF₆) as the supporting electrolyte at room temperature. The cyclic voltammograms were obtained at a scan rate of 50 mV/s. Glassy carbon was used as a working electrode material and a platinum wire was used as a counter electrode, and all potentials were recorded versus Ag/Ag⁺ as a reference electrode. The ESR measurements were performed on a Bruker-EMX EPR spectrometer at room temperature. Films of intrinsic polymers and doped polymers for EPR analysis were prepared by drying the solutions in EPR tubes in a

vacuum oven at 120 °C for 12 h. GIWAXS characterization of the thin films was performed at beamline 7.3.3 of the Advanced Light Source, Lawrence Berkeley National Laboratory (LBNL). The X-ray beam energy was 10 keV. The sample to detector distance was ~280 mm calibrated with Ag behenate and the incidence angle was 0.16° normalized by a photodiode. All the GIWAXS signals were recorded in Helium atmosphere using a 2D charge-coupled device (CCD) detector (Pilatus 2M) with a pixel size of 0.172 mm by 0.172 mm using x-rays with a wavelength of $\lambda = 1.24$ Å. The films of polymers and doped polymers were prepared by drop-casting the solution on silicon substrates, then annealed at 120 °C for 12 h, which was similar to the preparation for doped devices. AFM images were taken in tapping mode using a Dimensional 3100 AFM (Bruker Nano, Santa Barbara, CA). The images were visualized using the Nanoscope software (Bruker). The thickness of films was measured using KEYENCE VK-X100 Laser microscope with 3D and profile measurements.

OFET Film Fabrication and Characterization.

Organic field electric transistors (OFET) devices with a top-gate/bottom-contact (TGBC) configuration were fabricated using n⁺⁺-Si/SiO₂ (300 nm) substrates. The gold source and drain bottom electrodes were patterned by thermal evaporation on the SiO₂ surface. The substrates were subjected to cleaning using ultrasonication in cleaning agent, deionized water, acetone, and isopropanol. The cleaned substrates were dried under vacuum at 60 °C for 6 h and then transferred into a glovebox. Thin films of polymers and doped PNDICITVT and PBDOPVTT were prepared by spin coating the solution (4 and 2.5 mg/mL in orthodichlorobenzene (*o*-DCB)) on the treated substrates at 1500 rpm for 60 s and annealed at 160 °C for 20 min. Then, the solution of PMMA was spin-coated on the polymer films at 2000 rpm for 60 s and annealed at 100 °C for 2 h, resulting in a dielectric layer 1030 nm thick. Gate electrodes comprising a layer of

Au (50 nm) were then evaporated through a shadow mask onto the dielectric layer by thermal evaporation. The OFET devices had a channel length (L) of 200 μm and a channel width (W) of 8000 μm . Evaluations of the OFETs were carried out in atmosphere (humidity 40-65%) on a probe stage using Keithley 4200 and Agilent 4155C as parameter analyzers. The mobility was calculated in the saturation regime according to the equation: $I_{DS} = (W/2L)\mu C_i(V_G - V_T)^2$, where I_{DS} is the drain current, μ is the mobility, and V_G and V_T are the gate voltage and threshold voltage, respectively.

Thermoelectric devices and properties measurements.

Glass substrates (Corning Inc.) were cleaned by sonication in a cleaning agent, deionized water, acetone, and isopropanol. Gold electrodes (50 nm thick) were deposited on glass with a channel length of 3 mm and a channel width of 7 mm. Polymers and dopants were dissolved in *o*-DCB separately with the concentration of 4 for PNDICITVT, 2.5 for PBDOPVTT and 2.5 mg mL^{-1} , respectively. The polymer and the dopant solution were heated at 90 $^{\circ}\text{C}$ for 48 h. Then the polymer was blended with dopant to the desired concentration. The mixed solution was heated at 90 $^{\circ}\text{C}$ and stirred for 30 min. The final solution was dropped on the glass substrate on which 2D wells are fabricated by laying a pattern of Novec polymer. After natural evaporation of the solvent in a glove box over 60 h, square films form. The devices were annealed on a hot plate at 120 $^{\circ}\text{C}$ for 12 h in nitrogen. All the measurements were performed in open air (humidity 45-68%). Resistance was measured using a four-probe method with an Agilent 4155C Semiconductor Parameter Analyzer. At least three measurements of resistance were performed on each sample surface in different positions. The Seebeck coefficient can be calculated using the equation $S = \Delta V / \Delta T$, where ΔV is the thermal voltage obtained between the two electrodes of the device subjected to a temperature gradient ΔT . Three to six ΔT values were imposed on the sample, so that the slopes of ΔV versus ΔT give values of the Seebeck coefficient.

2. Figures and tables.

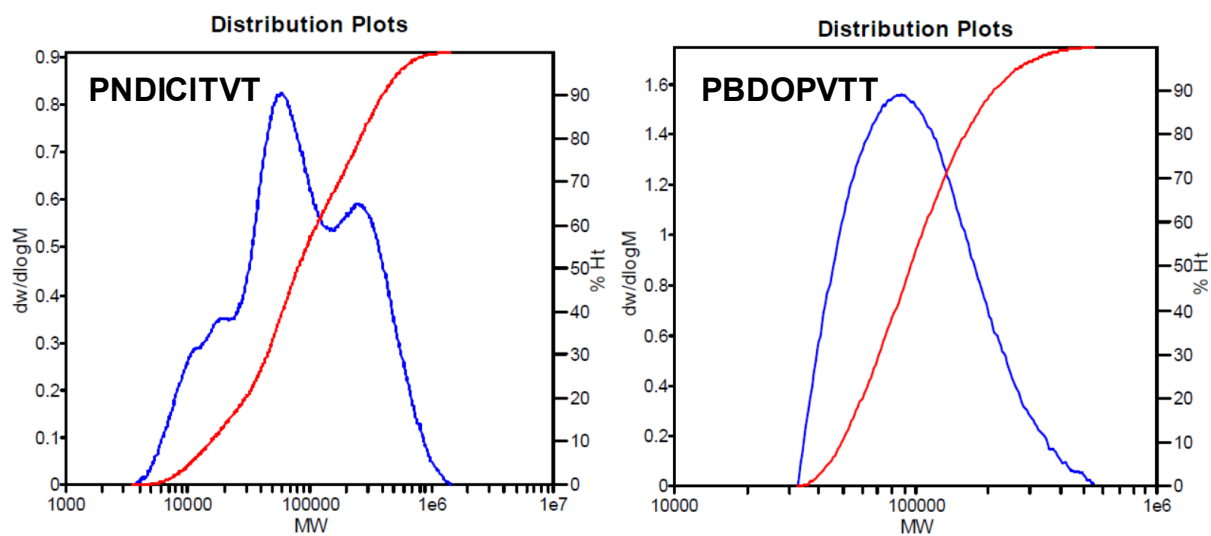


Figure S1. The GPC spectra of two polymers.

Table S1. Characters of polymers.

Polymer	M_n (kDa)	M_w (kDa)	PDI
PNDICITVT	41.3	153.8	3.7
PBDOPVTT	85.7	115.6	1.3

PD

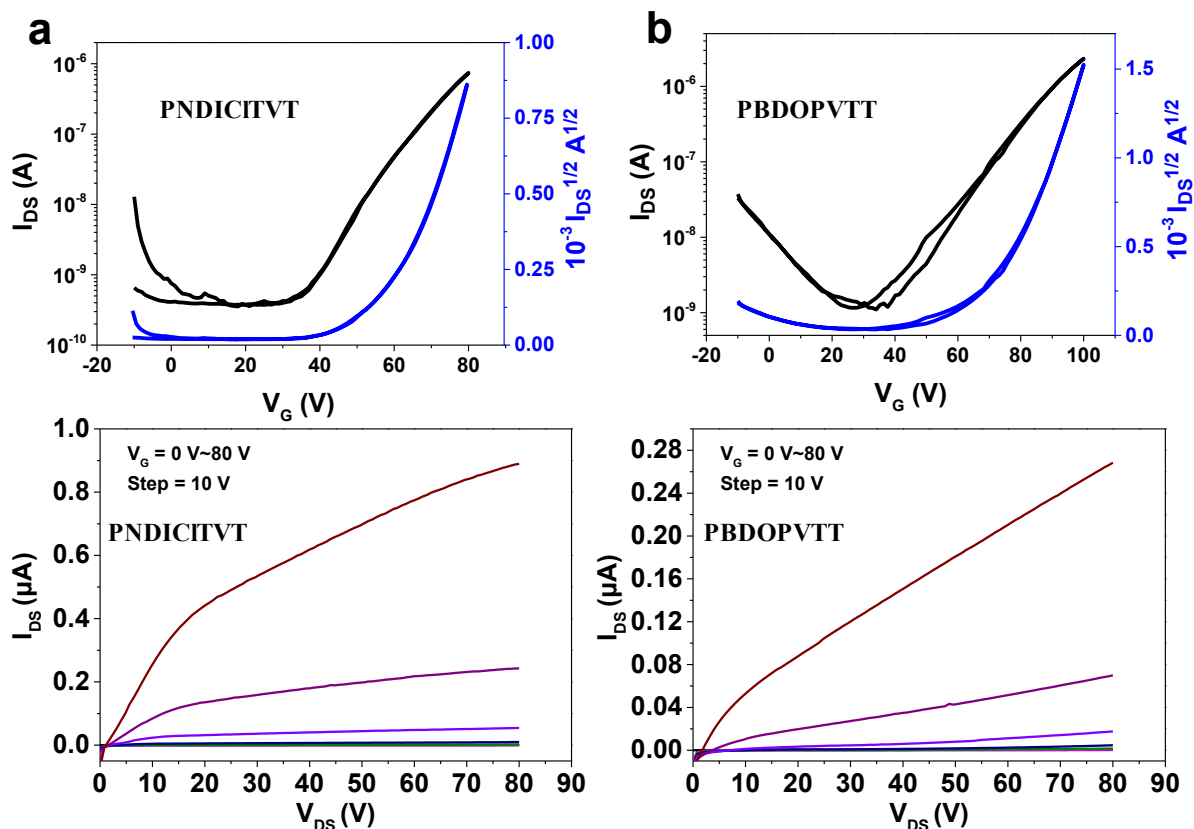


Figure S2. The transfer and output curves of (a) PNDICITVT and (b) PBDOPVTT.

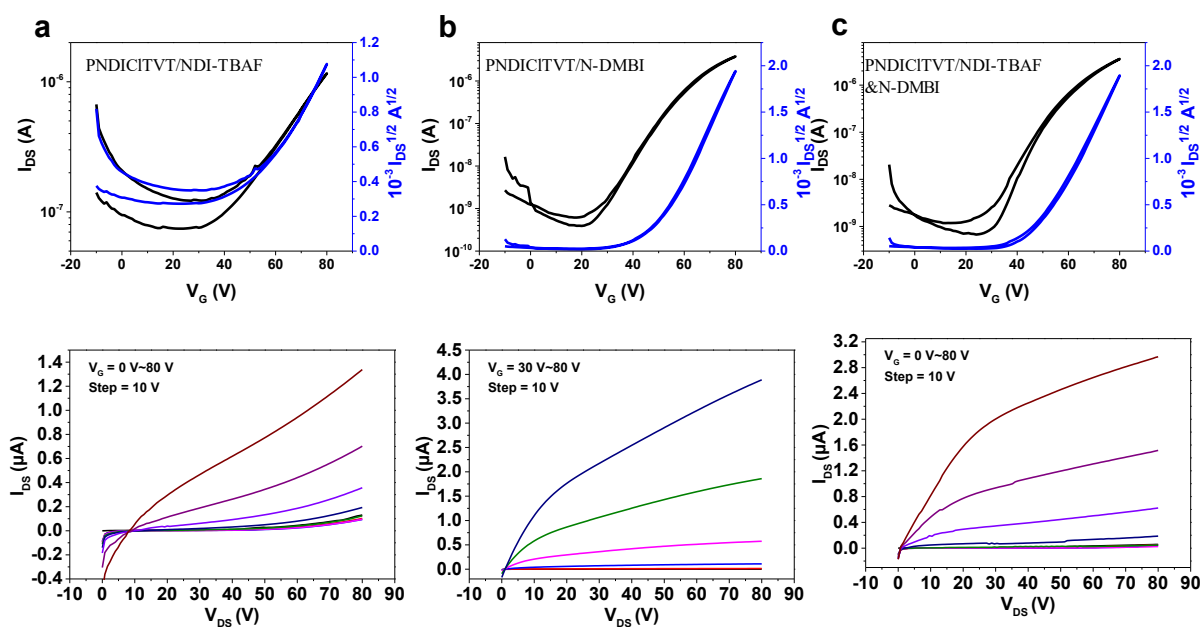


Figure S3. The transfer and output curves of PNDICITVT doped with (a) NDI-TBAF, (b) N-DMBI and (c) co-dopants of NDI-TBAF and N-DMBI.

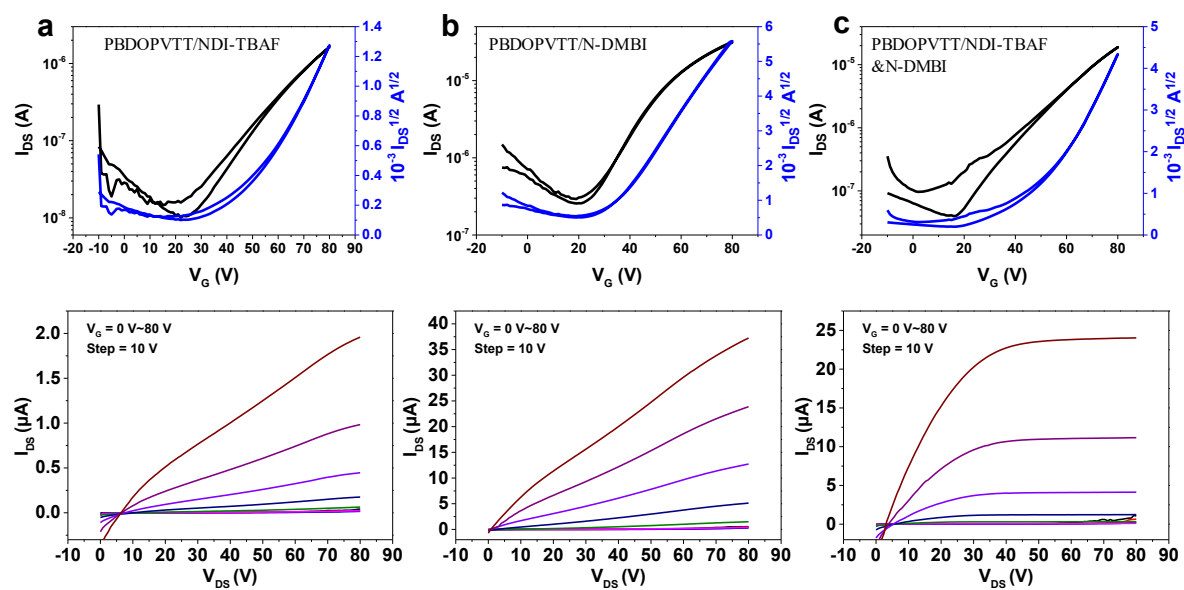


Figure S4. The transfer and output curves of PBDOPVTT doped with (a) NDI-TBAF, (b) N-DMBI and (c) co-dopants of NDI-TBAF and N-DMBI.

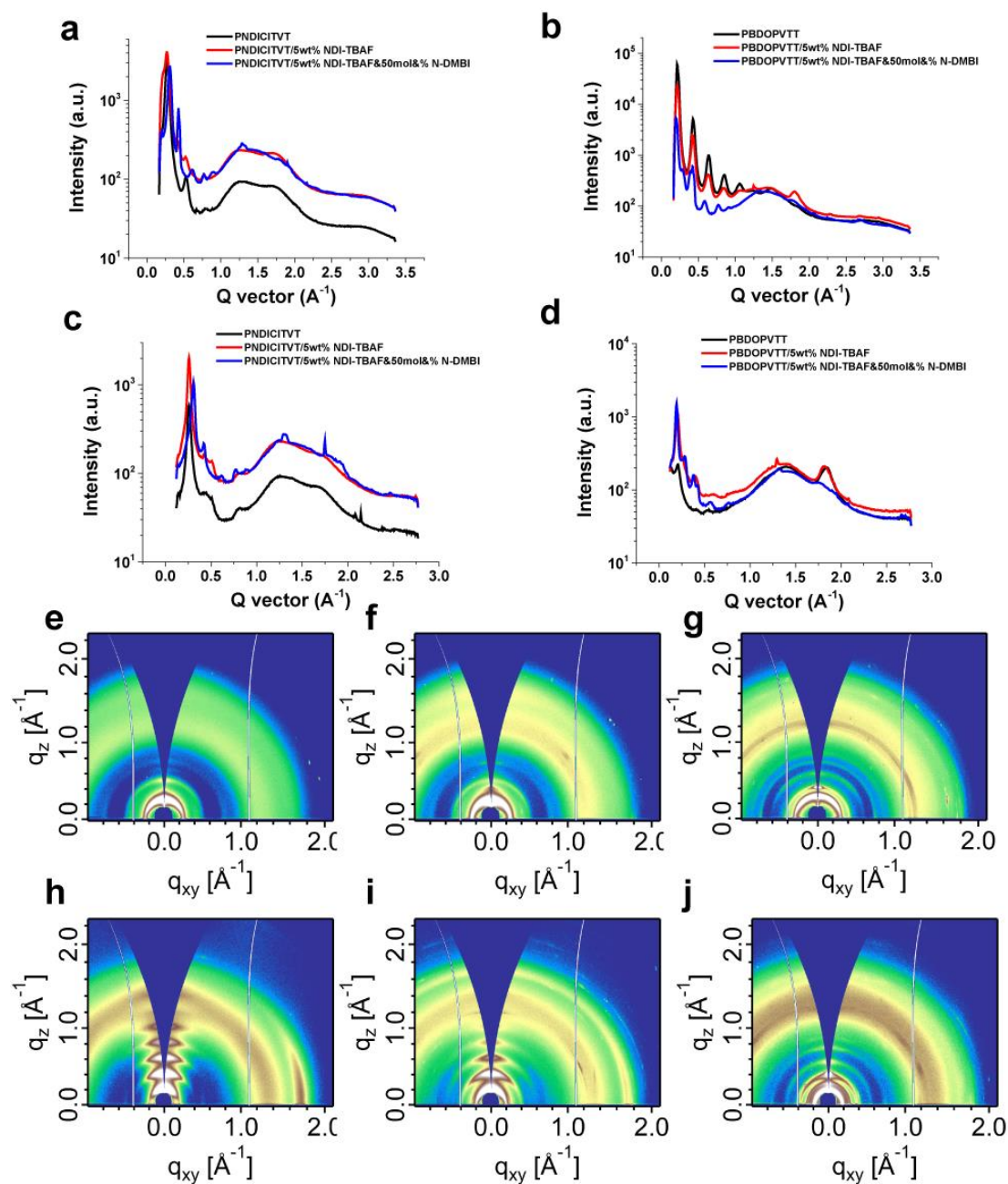


Figure S5. GIWAXS plots for doped and undoped polymers. (a) (b) Out-of-plane and (c) (d) in-plane curves of pristine and doped polymer films. GIWAXS spectra of (e) (h) pristine PNDICITVT (PBDOPVTT), PNDICITVT (PBDOPVTT) doped with (f) (i) NDI-TBAF and (g) (j) co-dopants of NDI-TBAF and N-DMBI.

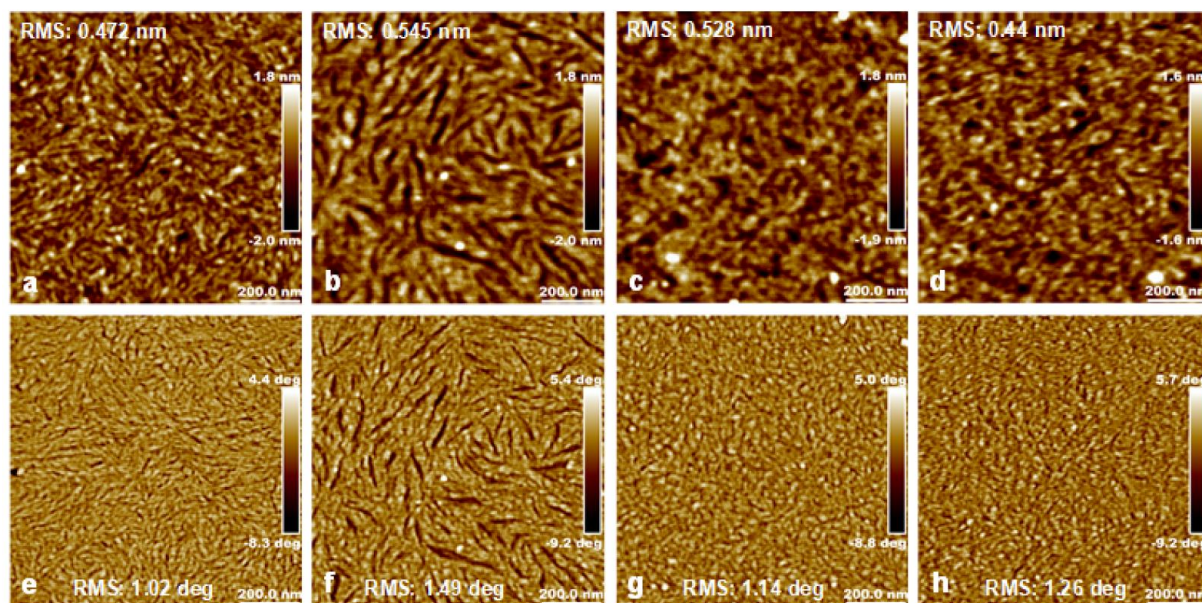


Figure S6. AFM height (phase) images of (a) (e) pristine, (b) (f) NDI-TBAF, (c) (g) N-DMBI and (d) (h) co-dopants of NDI-TBAF and N-DMBI doped PNDICITVT.

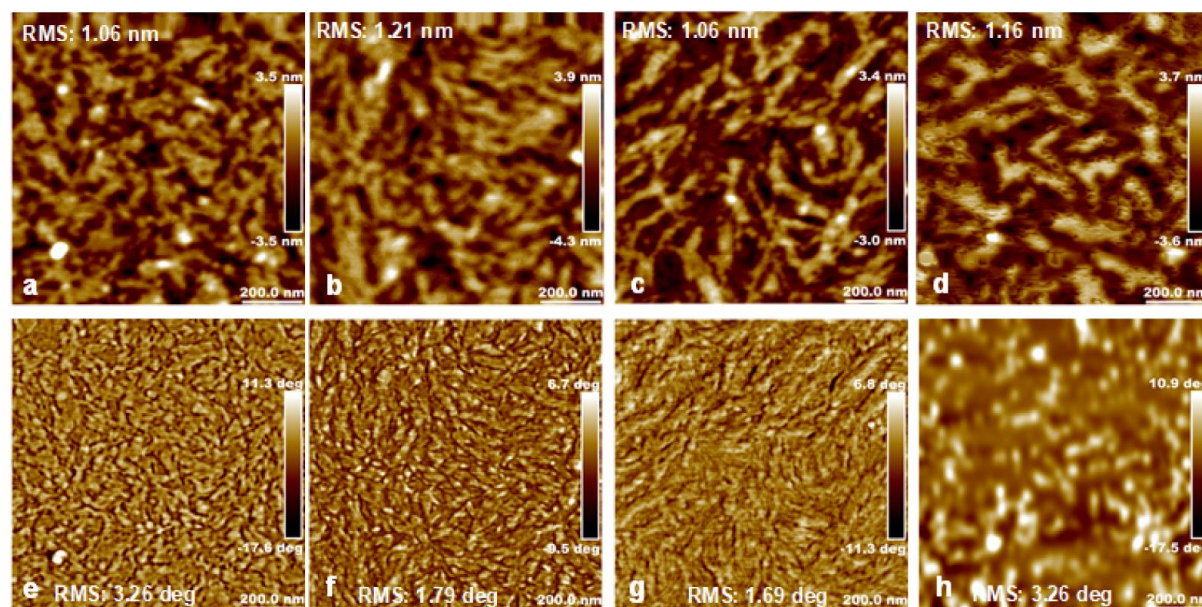


Figure S7. AFM height (phase) images of (a) (e) pristine, (b) (f) NDI-TBAF, (c) (g) N-DMBI and (d) (h) co-dopants of NDI-TBAF and N-DMBI doped PBDOPVTT.

3. Simulation details.

To allow the systems in this computational study to remain tractable while maintaining an acceptably rigorous level of theory, the chemical nature of the NDI-TBAF system (see Figure 1) was simplified while still remaining functionally accurate. To that end, the N-(2-octyl)dodecane functional groups on the imides were substituted by N-methane. While the fluoride ion present in TBAF remained the same throughout all simulations, the systems studied include: NDI with a bare fluoride ion, NDI with CsF, and NDI with TMAF. The “rasterization” process across different initial simulation structures involved placing a 4x4 grid of dopants (i.e. ions or ion pairs), one per structure, for 16 different structures, 3 nm above the area spanned by the NDI molecule. Figure S8 shows one such example for the bare fluoride ion simulations. The geometry optimization function within the ORCA software package was used to find the preferred locations in three dimensions of each ion or pair in these 16 separate simulations. The relevant molecular species were represented with a B97-D3 functional and def2-TZVP basis set, which we have used in the past, and which is recommended by Grimme^[1]. A conductor-like polarizable continuum solvation model (CPCM) was employed to simulate a homogeneous acetonitrile medium with dielectric constant $\epsilon = 36.6$. Each simulation was run with 4 processors on Haswell nodes and took roughly 2 hours of wall time.

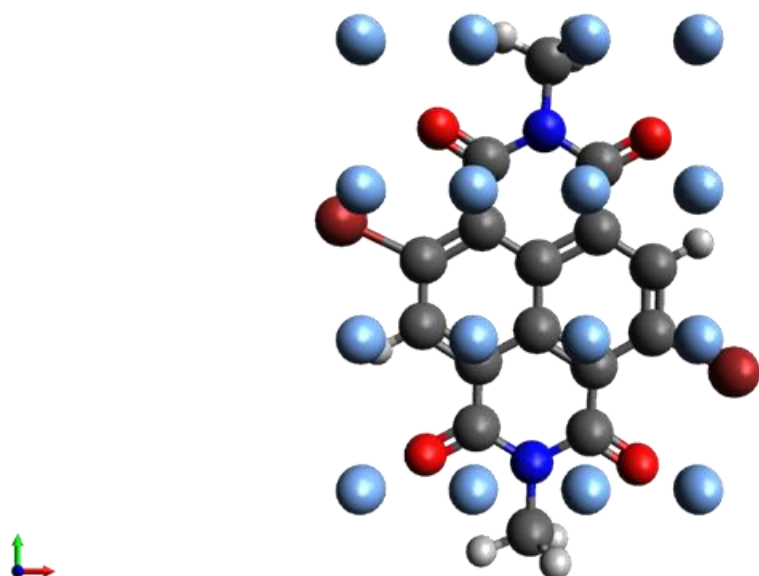


Figure S8. Initial locations of fluoride ions forming a total of 16 possible locations that raster across the surface of the NDI molecule.

Preferred locations of the fluoride ions coalesced onto 7 total locations, three of which were positionally unique, as shown in the main section of this manuscript. These were accepted to be the most favorable binding sites for a fluoride ion. Once the geometry-optimized fluoride ion locations were identified, single-point calculations at the same level of theory were conducted, with the system containing one less electron. The resulting difference corresponded to the ionization potential of the system, a technique similar to the one utilized in previous research by Jursic.^[2] A very similar process was then repeated for the simulations with CsF and TMAF. The main difference arose in an investigation of the positional variance of the counterion position around the fluoride ion. For the preferred sites identified with the bare fluoride ion simulations, counterions were initialized in four directions around the fluoride ions and then geometry-optimized in separate simulations. Figure S9 shows one such result from both the CsF (S9a) and TMAF (S9b) simulations.

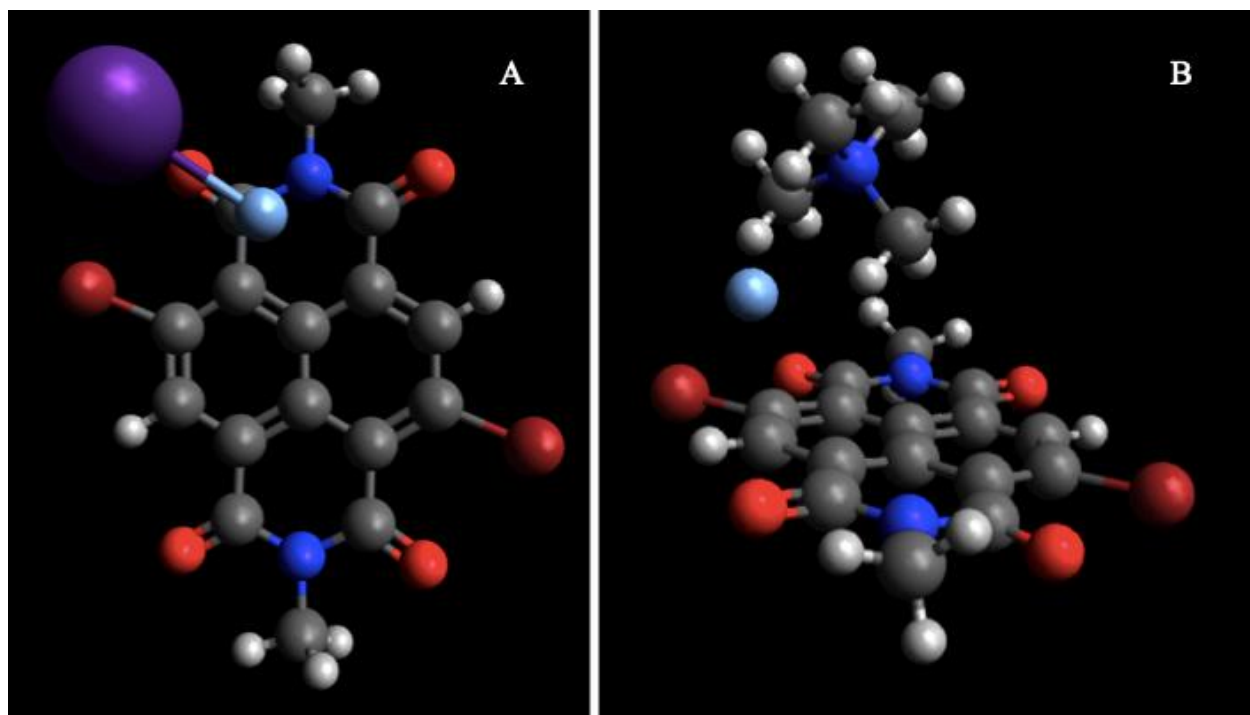
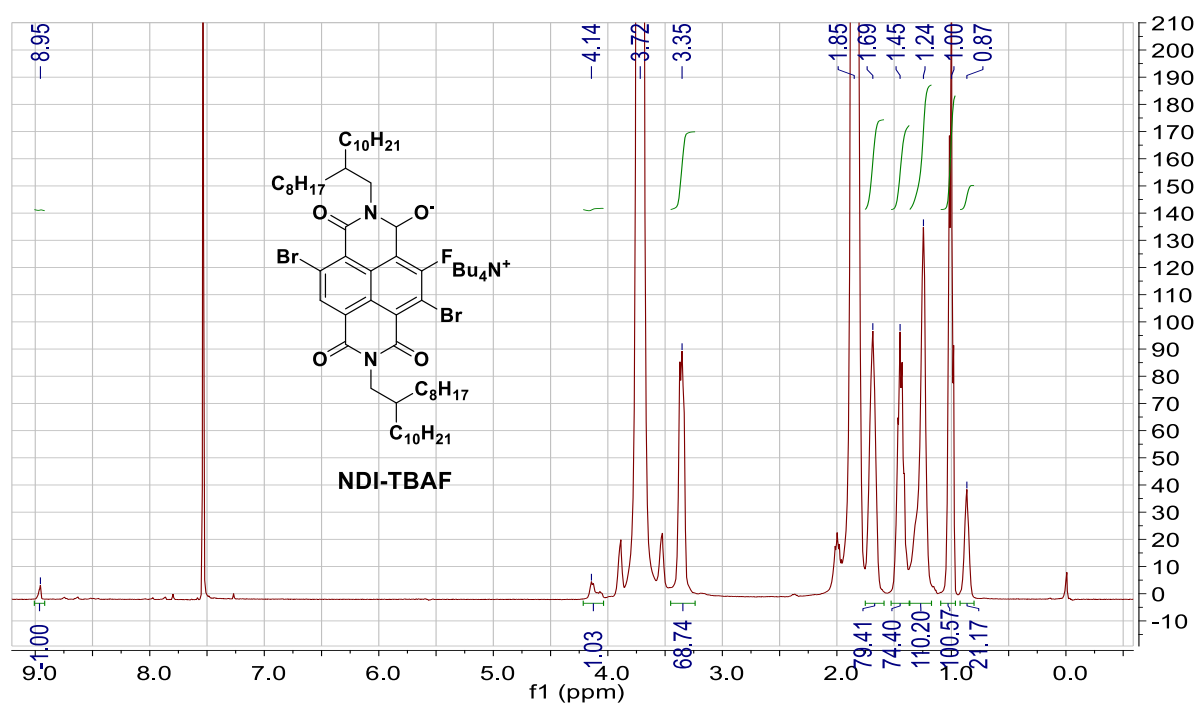
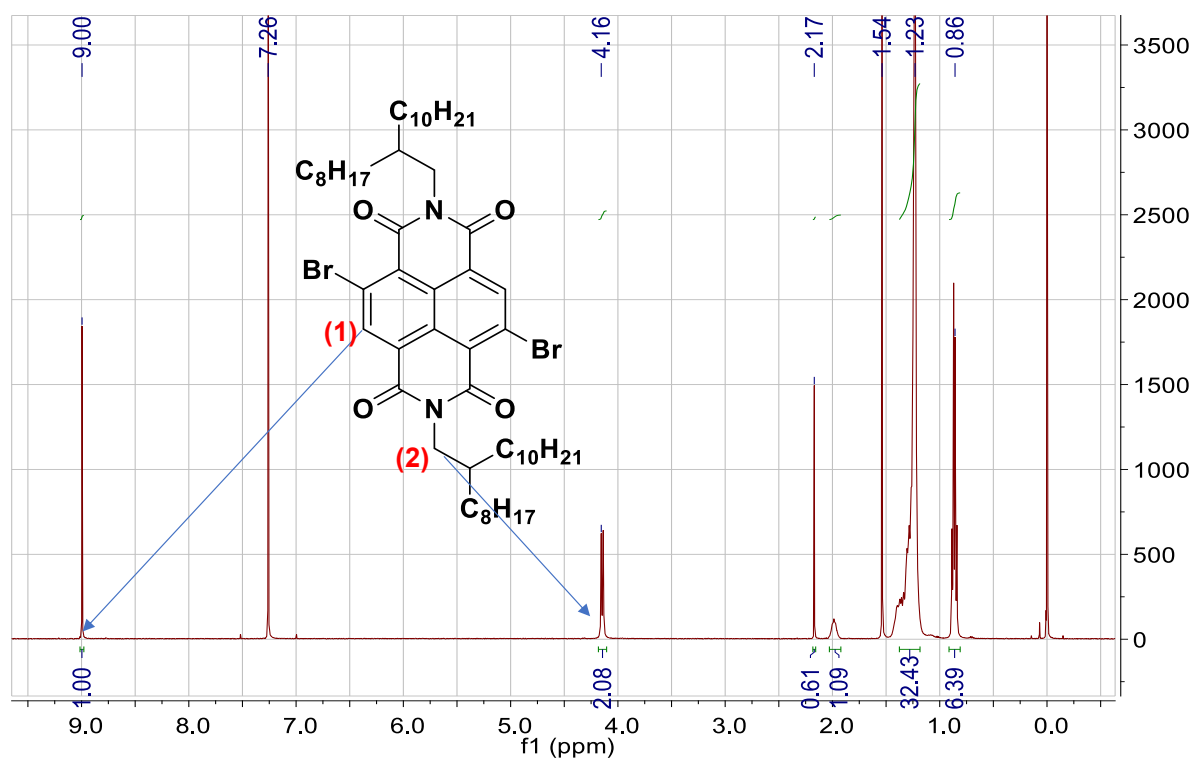
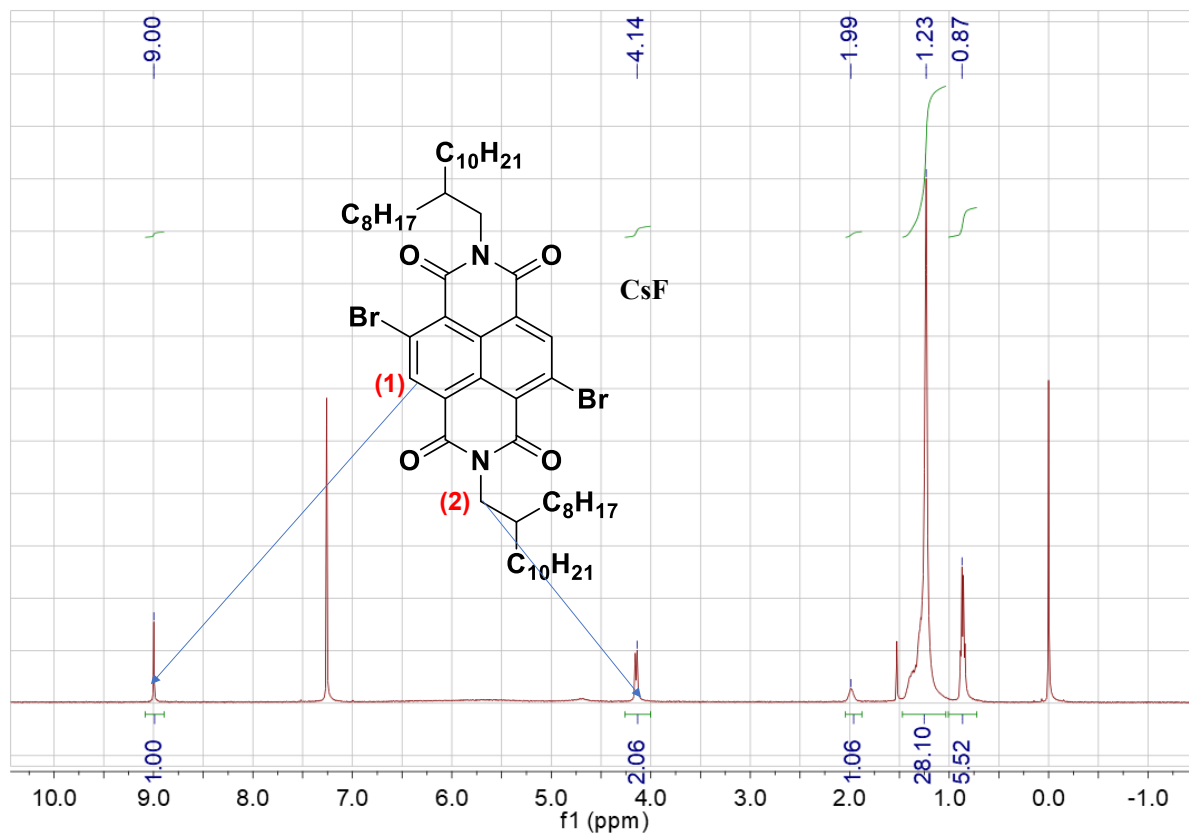


Figure S9. Geometry-optimized results of counterion dopant simulations. (A) CsF dopant. (B) TMAF dopant rotated for visual clarity.

4. NMR of NDI-2Br, NDI-TBAF and NDI:CsF.





As shown in the NMR spectra, the ratio of peak of aryl-H (1) with N-CH₂ (2) changes from NDI-2Br (1/2) to NDI-TBAF (1/1), and there are no changes of CsF's.

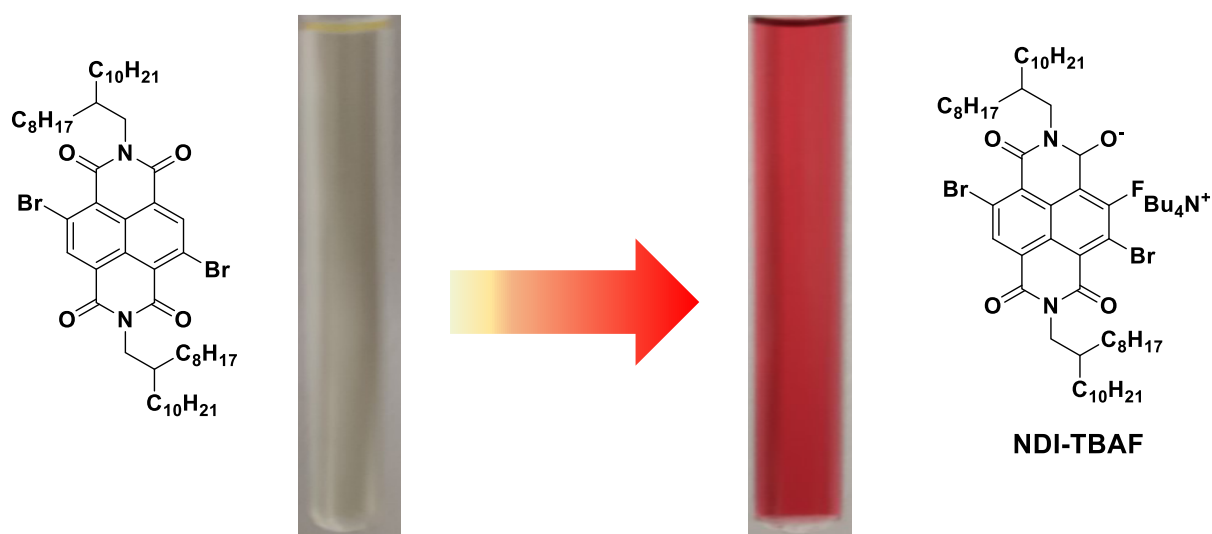


Figure S10. Color changes from NDI-2Br to NDI-TBAF.

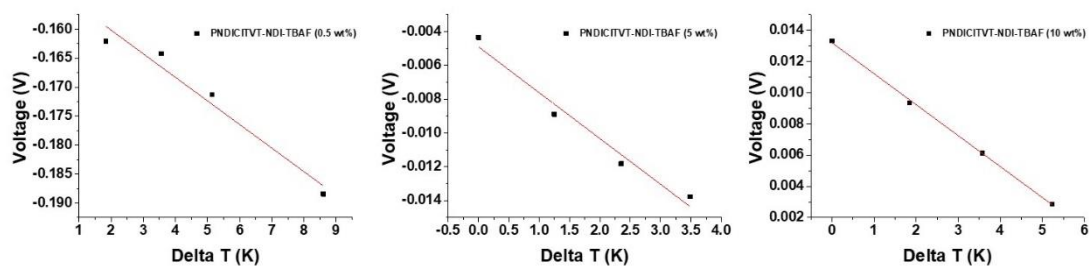


Figure S11. Slope determination of S (PNDICITVT doped with NDI-TBAF).

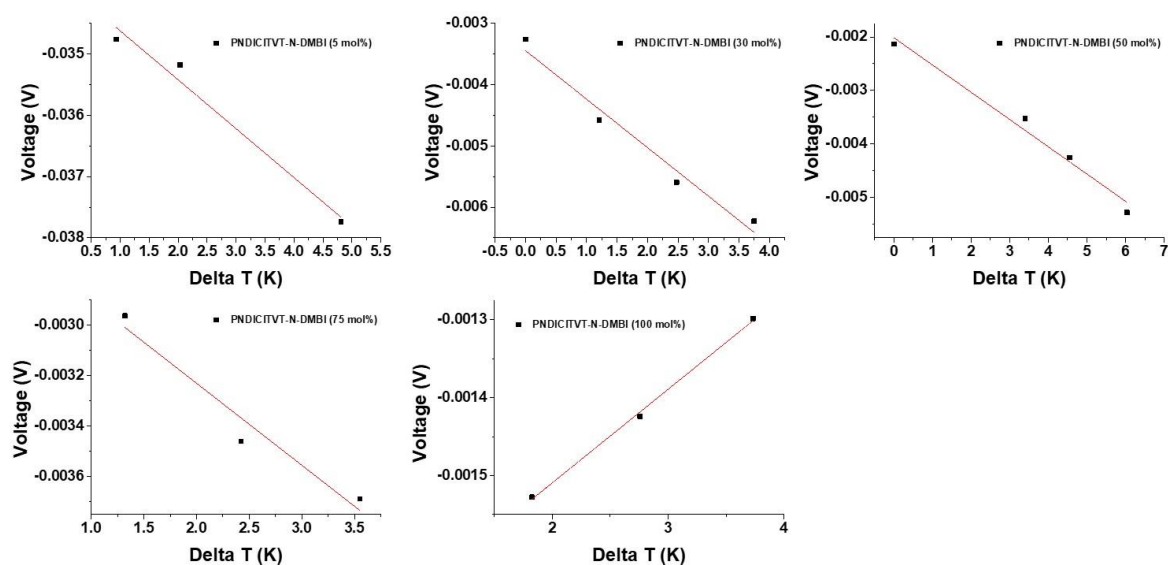


Figure S12. Slope determination of S (PNDICITVT doped with N-DMBI).

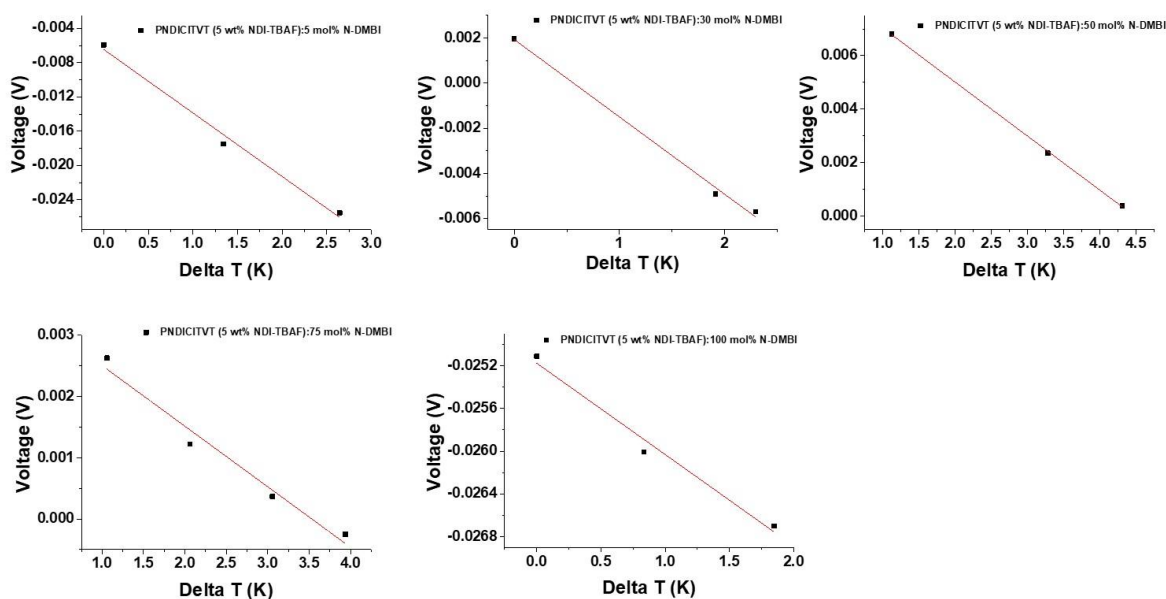


Figure S13. Slope determination of S (PNDICITVT doped with co-dopants).

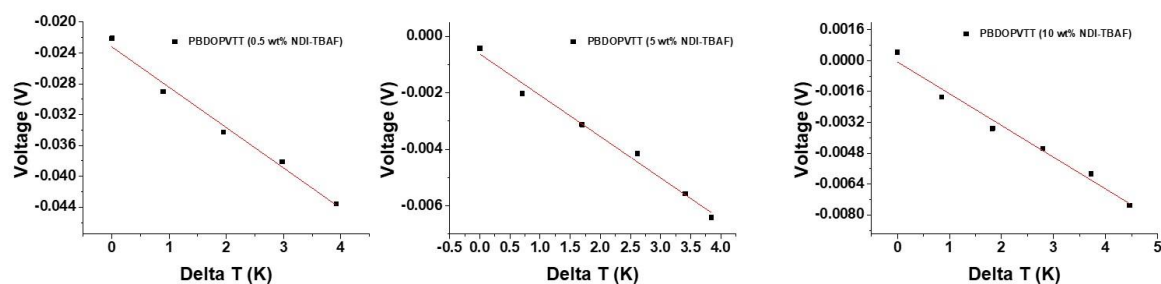


Figure S14. Slope determination of S (PBDOPVTT doped with NDI-TABF).

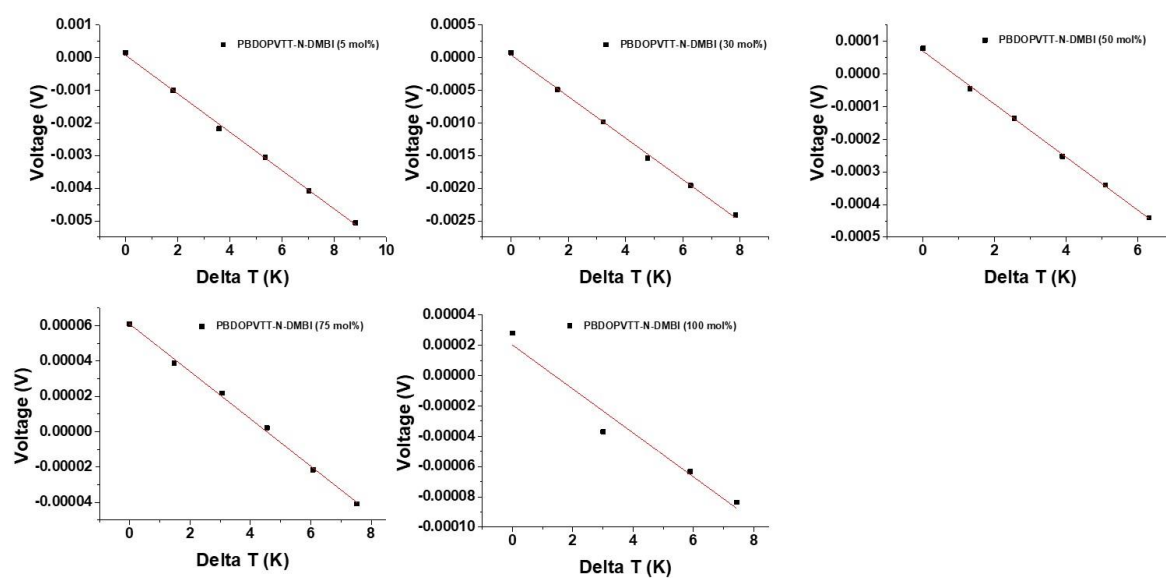


Figure S15. Slope determination of S (PBDOPVTT doped with N-DMBI).

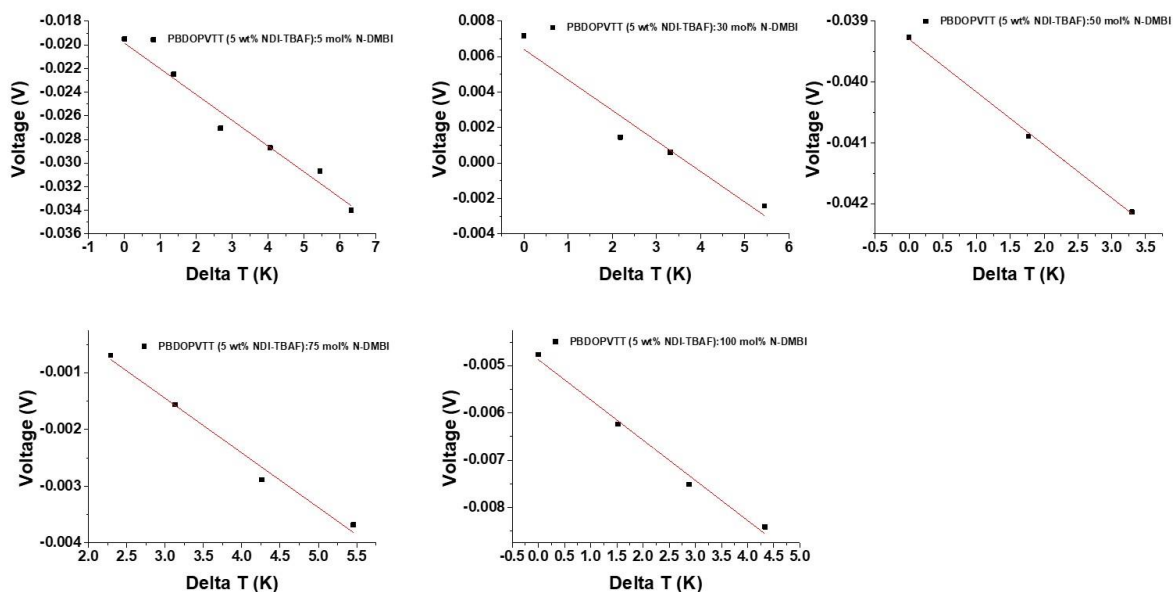
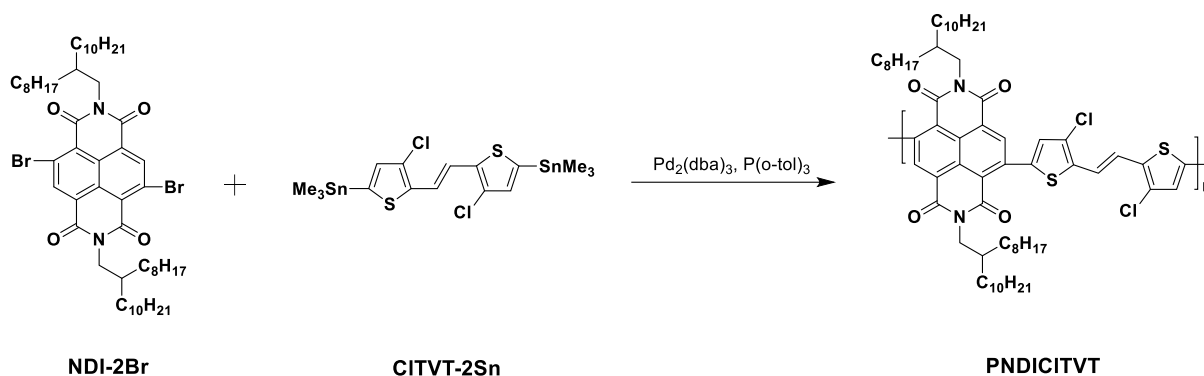


Figure S16. Slope determination of S (PBDOPVTT doped with co-dopants).

5. Synthesis of polymers.



CITVT-2Sn and PBDOPVTT was synthesized according to the references.^[1-3]

PNDICITVT:

Compound NDI-2Br (246.3 mg, 0.25 mmol) and CITVT-2Sn (146.7 mg, 0.25 mmol) were added to a dried Schlenk tube and moved to glove box (N_2 , $\text{H}_2\text{O} < 6$ ppm, $\text{O}_2 < 0.1$ ppm), anhydrous ortho-dichlorobenzene (3 mL), $\text{Pd}_2(\text{dba})_3$ (3 mg) and $\text{P}(\text{o-Tolyl})_3$ (5 mg) were added. The reaction medium was then stirred for 16 h at 130°C . Then 0.2 mL of bromobenzene was added to it after which stirring for further 12 h. After cooling to room temperature, the polymer was precipitated into methanol (300 mL) and filtered, then dried in vacuum drying oven. The polymer was washed in Soxhlet extractor with

acetone, hexane and dichloromethane overnight. The final product was dried under reduced pressure at 60 °C to obtain a black solid (86% yield). GPC: $M_n = 41.3$ kDa, $M_w = 153.8$ kDa, $PDI = 3.7$.

6. Steadiness of Seebeck measurements

We measured voltage differences induced by 3-5 different temperature differences during successive time intervals of several minutes each, with the total measurement time of 18 minutes or more. Voltage differences were averages of eight raw voltage measurements at an individual temperature; these raw voltages typically varied randomly by about 10-20%. Seebeck coefficients calculated from data from the individual temperatures were consistent with each other to within 10-15%, except for two less consistent points taken at the lowest and least certain temperature differences of <2 K.

References:

- [1] L. Goerigk, S. Grimme, *Phys. Chem. Chem. Phys.* **2011**, *13*, 6670.
- [2] B. Jursic, *J. Mol. Struct. THEOCHEM.* **1998**, *452*, 145.
- [3] J. Han, H. Fan, Q. Zhang, Q. Hu, T. P. Russell, H. E. Katz, *Adv. Func. Mater.* **2020**, doi:10.1002/adfm.202005901.
- [4] Y.-Q. Zheng, Z.-F. Yao, T. Lei, J.-H. Dou, C.-Y. Yang, L. Zou, X. Meng, W. Ma, J.-Y. Wang, J. Pei, *Adv. Mater.* **2017**, *29*, 1701072.
- [5] Zhao, X., Madan, D., Cheng, Y., Zhou, J., Li, H., Thon, S. M., Bragg, A. E., DeCoster, M. E., Hopkins, P. E., Katz, H. E., *Adv. Mater.* **2017**, *29*, 1606928.